

Singular low-energy states of tilted Dirac semimetals induced by the fermion-fermion interactions

Jie-Qiong Li, Dong-Xing Zheng, and Jing Wang*

Department of Physics, Tianjin University, Tianjin 300072, P.R. China

(Dated: February 2, 2022)

We attentively investigate the effects of short-range fermion-fermion interactions on the low-energy properties of both two-dimensional type-I and type-II tilted Dirac semimetals by means of the renormalization group framework. Practicing the standard renormalization group procedures via taking into account all one-loop corrections gives rise to the coupled energy-dependent evolutions of all interaction parameters, which are adopted to carefully examine whether and how the fermion-fermion interactions influence the low-energy physical behaviors of tilted Dirac fermions. After carrying out the detailed analysis of coupled flows, we figure out the tilting parameter dictates the low-energy states of tilted Dirac fermions in conjunction with starting values of fermion-fermion couplings. With proper variations of these two kinds of parameters, the tilted Dirac fermions can either flow towards the Gaussian fixed point or undergo certain instability that is conventionally accompanied by a phase transition in the low-energy regime. In addition, all potential instabilities can be clustered into five distinct classes owing to the competitions between the tilting parameter and initial fermionic interactions. Moreover, the dominant phases accompanied by the instabilities are determined via computing and comparing the susceptibilities of eight potential phases.

I. INTRODUCTION

Both electronic states and physical properties of Dirac materials including two-dimensional (2D) graphene [1–4], Weyl semimetals (WSMs) [5–13], and Dirac semimetals (DSMs) [14–27] have been poured extensively attention in the contemporary condensed matter physics. In a sharp contrast to the conventional Fermi metals featuring a finite Fermi surface [28], they generally only possess discrete Dirac nodal points and exhibit a linear quasiparticle dispersion with gapless low-energy excitations [3, 14, 15]. As a result, the density of states (DOS) vanishes at Dirac points [3, 14] and then induces a multitude of interesting phenomena including non-trivial topological properties [29, 30] and non-centrosymmetric WSMs with time-reversal protected states [9–11, 31–34]. It is of remarkable significance to highlight that Dirac/Weyl cones can be stretched and thus tilted by breaking the fundamental Lorentz symmetry with additional forces [35, 36] or so-called t -Lorentz symmetry [37]. In other words, this is equivalent to inducing anisotropic fermion velocities of energy dispersions for DSMs and/or WSMs.

Recently, tilted Dirac materials have attracted considerable attention in condensed matter fields. For instance, tilted Dirac cones have been realized in the two-dimensional (2D) organic compound α -(BEDT-TTF)₂I₃ and certain mechanically deformed graphene [38–40]. In addition, the three-dimensional (3D) tilted Weyl cones have been proposed in WTe₂ [41], the Fulde-Ferrell ground state of a spin-orbit coupled fermionic superfluid [42], or a cold-atom optical lattice [43]. All these kinds of materials are therefore designated as tilted DSMs (WSMs), which conventionally can

be broken into two distinct types relying heavily upon the tilted angles. Type-I tilted DSMs (WSMs) still maintain analogous Dirac (Weyl) cones as long as the tilted angle is insufficient to destroy the point-like Fermi surface [3, 4, 44]. In comparison, the nodal point would be replaced by two straight lines indicating the open Fermi surface and nonzero DOS, once the tilted angle is adequately large [35]. We therefore obtain another breed of tilted materials dubbed type-II tilted DSMs (WSMs) [41], which have been recently realized in both PdTe₂ [45, 46] and PtTe₂ [47].

Attesting to unique Dirac cones and unconventional low-energy excitations of tilted DSMs, they become one of the hottest topics in condensed matter physics [35, 36, 48–63]. In particular, the effects of long-range Coulomb interactions on the low-energy properties of tilted DSMs were investigated by many groups [35, 36, 54, 55]. Unfortunately, it is well known that the long-range Coulomb interaction would be easily screened in the realistic systems by adopting some metallic substrate to enhance the dielectric constant [3, 64–66]. Accordingly, the short-range fermion-fermion interactions, which can induce a plethora of unusual behaviors in fermionic systems [67–71], tend to play a vital role in pinning down the low-energy physical implications once the Coulomb interaction is screened in the realistic or excluded by external forces [3, 64–66]. However, the fermion-fermion interactions are hitherto inadequately taken into account in previous studies of 2D tilted DSMs. This indicates the physical information that is closely associated with these locally fermionic interactions may be partially discarded or cannot be fully captured in the low-energy regime. In order to improve our understandings for these tilted materials, it is therefore considerably instructive to carefully investigate whether and how the fermion-fermion interactions affect the low-energy physical properties of the 2D tilted DSMs?

*Corresponding author: jing.wang@tju.edu.cn

Stimulated by these, we within this work endeavor to explore how four distinct sorts of short-range fermion-fermion interactions affect the low-energy fates of physical states for 2D type-I and type-II tilted-Dirac materials. In order to treat all types of these fermion-fermion interactions on the same footing, it is convenient to adopt the powerful energy-shell renormalization group (RG) approach [72–74]. Performing all one-loop calculations and carrying out the standard RG analysis give rise to the entangled RG evolutions, which are closely associated with all interaction parameters and thus carry the full physical information. Several interesting physical behaviors have been extracted from these coupled RG equations.

To be concrete, we realize that the low-energy states of tilted DSMs are sensitive to both the tilting parameter ζ and initial values of fermion-fermion interactions that are characterized by $|\lambda_i(0)|$ with $i = 0, 1, 2, 3$ (in order to facilitate our analysis, we exploit $\lambda_i(0)$ hereafter to denote $|\lambda_i(0)|$ with $i = 0, 1, 2, 3$) corresponding to different sorts of fermionic interactions. Tuning the values of ζ and $\lambda_i(0)$, the tilted DSMs can be attracted and flow to the Gaussian fixed point or certain instability associated with some phase transition at a critical energy scale. For type-I DSMs, both the increase of ζ and $|\lambda_i(0)|$ would be helpful to activate an instability in the low-energy regime. In comparison, the increase of $|\lambda_i(0)|$ is in favor to trigger certain potential instability for type-II tilted DSMs but instead tuning up ζ is harmful to the development of instability. In addition, these two quantities ζ and $|\lambda_i(0)|$ strongly compete and exhibit different powers in both type-I and type-II DSMs attesting to qualitatively different topologies of Fermi surfaces. For the type-I tilted DSMs, $|\lambda_i(0)|$ plays a major role in pinning down the low-energy states except $\zeta \rightarrow 1$ at which ζ is responsible for the possible instability. Whereas, the tilting parameter ζ dominates the low-energy fates of the type-II tilted DSMs once ζ is sufficient large and instead $|\lambda_i(0)|$ wins the competition if ζ is small or $\zeta \rightarrow 1$. Furthermore, we figure out that all underlying instabilities that are induced in both type-I and type-II tilted DSMs can be divided into five different classes depending on both the interplays among fermion-fermion interactions and tilting parameter in the low-energy regime. Specifically, four classes of instabilities can be expected in the type-I tilted system. Rather, the type-II tilted Dirac fermions allow two distinct classes of instabilities. The basic results for type-I and type-II tilted Dirac fermions are provided in Table I and Table II, respectively. At last, we show that ferromagnet, antiferromagnet, and spin bond density are more preferable in the vicinity of these instabilities after evaluating and comparing the susceptibilities of potential phases.

The rest of this paper is structured as follows. In Sec. II, we introduce our microscopic model and the related effective quantum field theory. The Sec. III is accompanied to compute all the one-loop corrections to the interaction parameters, which are utilized to derive the coupled flow equations via performing the standard RG analysis. We provide detailed analysis of singular low-

energy states caused by the fermion-fermion interactions for type-I and type-II tilted Dirac fermions in Sec. IV and Sec. V, respectively. In Sec. VI, we divide all underlying instabilities induced by fermion-fermion interactions into five distinguished classes depending upon the specific values of both tilting parameter and starting values of fermionic couplings and address the dominant phases around all the potential instabilities. Finally, we provide a brief summary of our primary results in Sec. VII.

II. EFFECTIVE THEORY

Within this work, we focus on the 2D tilted DSMs at the chemical potential $\mu = 0$, whose non-interacting effective action in the low-energy regime can be written as [35, 40]

$$S_0 = \sum_{\xi, \alpha} \int \frac{dp_0}{2\pi} \int \frac{d^2\mathbf{p}}{(2\pi)^2} \psi_{\xi\alpha}^\dagger(p_0, \mathbf{p}) (-ip_0 + \xi\zeta v_1 p_1 + \xi v_1 p_1 \sigma_1 + p_2 \sigma_2) \psi_{\xi\alpha}(p_0, \mathbf{p}), \quad (1)$$

with the valley degeneracy $\xi = \pm 1$, spin degeneracy $\alpha = \pm 1$, and Pauli matrices σ_i satisfying the anticommutation algebra $\{\sigma_i, \sigma_j\} = 2\delta_{ij}$ ($i, j = 1, 2, 3$). Here, the fermionic spinors $\psi_{\xi\alpha}(p_0, \mathbf{p})$ and $\psi_{\xi\alpha}^\dagger(p_0, \mathbf{p})$ are exploited to characterize the excited quasiparticles around the nodal points at \mathbf{K} ($-\mathbf{K}$) in the first Brillouin zone. The dimensionless parameter ζ that is served as a tilting variable is able to tilt the Dirac cones and reshape the structure of Fermi surface as long as ζ is nonzero. As a result, it gives rises to two inequivalent fermion velocities v_1 and v_2 along the x and y directions, respectively.

Subsequently, one can straightforwardly extract the free fermionic propagator from the non-interacting action, namely

$$G_0(ip_0, \mathbf{p}) = \frac{1}{-ip_0 + \xi\zeta v_1 p_1 + \xi v_1 p_1 \sigma_1 + p_2 \sigma_2}. \quad (2)$$

With the help of this free action (1), the energy eigenvalues can be derived as follows,

$$\epsilon_{\pm}(\mathbf{p}) = \xi\zeta(v_1 p_1) \pm \sqrt{(v_1 p_1)^2 + (v_2 p_2)^2}, \quad (3)$$

which intimately hinge upon the value of ζ and principally govern the overall structure of Fermi surface. As a consequence, tilted DSMs can be manifestly clustered into distinct sorts via tuning the tilting parameter ζ [35]. At $|\zeta| < 1$, the DSMs still possess a point-like Fermi surface only with simply tilted Dirac cones and thus belong to the type-I Dirac systems. In sharp comparison, $|\zeta| > 1$ would completely sabotage the point-like structure of Fermi surface and yield an open Fermi surface that consists of two crossed lines, namely $(v_2 p_2) = \pm\sqrt{\zeta^2 - 1}(v_1 p_1)$ [35, 36]. Under such circumstance, it goes to the type-II Dirac systems.

To proceed, we would like to bear in mind that the primary concern of this work is to examine the low-energy

behaviors of both two-dimensional type-I and type-II tilted Dirac semimetals against fermion-fermion interactions. For this purpose, we are going to bring out the

four potential sorts of short-range fermion-fermion interactions [75–77],

$$S_{\text{int}} = \sum_{i=0}^3 \sum_{\alpha, \xi, \alpha', \xi'} \lambda_i \int_{-\infty}^{+\infty} \frac{dp'_0 dp''_0 dp'''_0}{(2\pi)^3} \int \frac{d^2\mathbf{p}' d^2\mathbf{p}'' d^2\mathbf{p}'''}{(2\pi)^6} \psi_{\xi\alpha}^\dagger(p'_0, \mathbf{p}') \sigma_i \psi_{\xi\alpha}(p''_0, \mathbf{p}'') \psi_{\xi'\alpha'}^\dagger(p'''_0, \mathbf{p}''') \sigma_i \psi_{\xi'\alpha'}(p'_0 + p''_0 - p'''_0, \mathbf{p}' + \mathbf{p}'' - \mathbf{p}'''), \quad (4)$$

where the coupling λ_i combined with its corresponding Pauli matrix σ_i are exploited together to designate certain breed of fermion-fermion interaction. For completeness, we run i from 0 to 3 and hence collect four distinct types of fermionic interactions.

At this stage, we are left with the effective theory after taking into account the non-interacting action (1) in tandem with fermionic interactions (4),

$$S_{\text{eff}} = S_0(p_j \rightarrow \tilde{p}_j/v_j) + S_{\text{int}}(p_j \rightarrow \tilde{p}_j/v_j), \quad (5)$$

where the index $j = 1, 2$. In order to simplify our notions and further analysis, we hereafter introduce two reduced momenta $\tilde{p}_1 \equiv v_1 p_1$ and $\tilde{p}_2 \equiv v_2 p_2$ to our effective theory. Based on this effective theory, we are going to study the low-energy properties under the presences of potential short-range fermion-fermion interactions and the competitions among them.

III. RG EVOLUTIONS

As aforementioned in Sec. II, the Fermi surfaces of 2D tilted DSMs can either be closed or open relying closely upon the concrete value of tilting parameter. Generally, following the spirit of RG approach [74], one can practice the RG process by eliminating and reshaping the thin momentum shells to approach the Fermi surface and construct the RG evolutions of related parameters for certain physical system, whose Fermi surface is well-defined (finite) and closed [28]. Based on the unusual structures of tilted Dirac fermions, we are now forced to give up momentum-shell RG but instead implement energy-shell RG. It implies that one needs to integrate out a thin energy shell one by one during the RG analysis [35, 74, 78–80].

In order to work in the energy-shell framework, we hereby parallel the strategies advocated in Ref. [35] and keep in mind the difference of energy dispersions between type-I and type-II tilted DSMs, whose equal-energy curves correspond to ellipses and hyperbolas, respectively. As a result, one is required to parametrize these two distinct sorts of equal-energy curves separately. To this end, we exploit the following transformations

from $(\tilde{p}_1, \tilde{p}_2)$ with $\tilde{p}_i = v_i p_i$ to (E, θ) [35, 36],

$$\text{Type-I: } \tilde{p}_1 = \frac{|E| \cos \theta - \xi \zeta E}{1 - \zeta^2}, \tilde{p}_2 = \frac{|E| \sin \theta}{\sqrt{1 - \zeta^2}}, \quad (6)$$

$$\text{Type-II: } \tilde{p}_1 = \frac{\xi \zeta E \pm |E| \cosh \theta}{\zeta^2 - 1}, \tilde{p}_2 = \frac{|E| \sinh \theta}{\sqrt{\zeta^2 - 1}}, \quad (7)$$

where E and θ designate the eigenvalues of energy $\epsilon_{\pm}(\mathbf{p})$ (3) and “effective angle” between \tilde{p}_1 and \tilde{p}_2 . Owing to qualitative distinctions of equal-energy curves between type-I and type-II tilted Dirac fermions, it is therefore worth pointing out that the variable θ at certain E is restricted to $0 \leq \theta < 2\pi$ and $-\infty < \theta < \infty$ for type-I and type-II situations, respectively. To proceed, we exploit the following Jacobian transformation $d\tilde{p}_1 d\tilde{p}_2 = |J| dE d\theta$ at $E > 0$ (the results for $E < 0$ can be obtained similarly),

$$J_{\text{type-I}} = \begin{vmatrix} \frac{\partial \tilde{p}_1}{\partial E} & \frac{\partial \tilde{p}_1}{\partial \theta} \\ \frac{\partial \tilde{p}_2}{\partial E} & \frac{\partial \tilde{p}_2}{\partial \theta} \end{vmatrix} = \begin{vmatrix} \frac{\cos \theta - \xi \zeta}{1 - \zeta^2} & -\frac{E \sin \theta}{1 - \zeta^2} \\ \frac{\sin \theta}{\sqrt{1 - \zeta^2}} & \frac{E \cos \theta}{\sqrt{1 - \zeta^2}} \end{vmatrix}, \quad (8)$$

$$J_{\text{type-II}} = \begin{vmatrix} \frac{\partial \tilde{p}_1}{\partial E} & \frac{\partial \tilde{p}_1}{\partial \theta} \\ \frac{\partial \tilde{p}_2}{\partial E} & \frac{\partial \tilde{p}_2}{\partial \theta} \end{vmatrix} = \begin{vmatrix} \frac{\cosh \theta \pm \xi \zeta}{\zeta^2 - 1} & \pm \frac{E \sinh \theta}{\zeta^2 - 1} \\ \frac{\sinh \theta}{\sqrt{\zeta^2 - 1}} & \frac{E \cosh \theta}{\sqrt{\zeta^2 - 1}} \end{vmatrix}, \quad (9)$$

Based on these the momentum integrals in the effective action (5) are accordingly casted into [35, 36]

$$\int_{\text{Type-I}} d^2\tilde{\mathbf{p}} = \frac{1}{2} \int_{-\Lambda}^{\Lambda} \frac{|E| dE}{(1 - \zeta^2)^{\frac{3}{2}}} \int_0^{2\pi} d\theta (1 - \eta_E \xi \zeta \cos \theta), \quad (10)$$

$$\int_{\text{Type-II}} d^2\tilde{\mathbf{p}} = \frac{1}{2} \int_{-\Lambda}^{\Lambda} \frac{|E| dE}{(\zeta^2 - 1)^{\frac{3}{2}}} \left[\int_{-\infty}^{\infty} d\theta (|\zeta| \cosh \theta + \eta_E \eta_{\zeta} \xi) + \int_{-\infty}^{\infty} d\theta (|\zeta| \cosh \theta - \eta_E \eta_{\zeta} \xi) \right]. \quad (11)$$

Here, integrals over θ for a fixed E in (10) and (11) denote the ellipse and the left (or right) branch of equal-energy hyperbola for type-I and type-II cases, respectively. In addition, the η_X with $X = E, \zeta$ collects the signs of E and ζ , namely $\eta_X \equiv \text{sgn}(X)$. Moreover, the parameter Λ characterizes the ultra cutoff that is directly associated with the lattice constant.

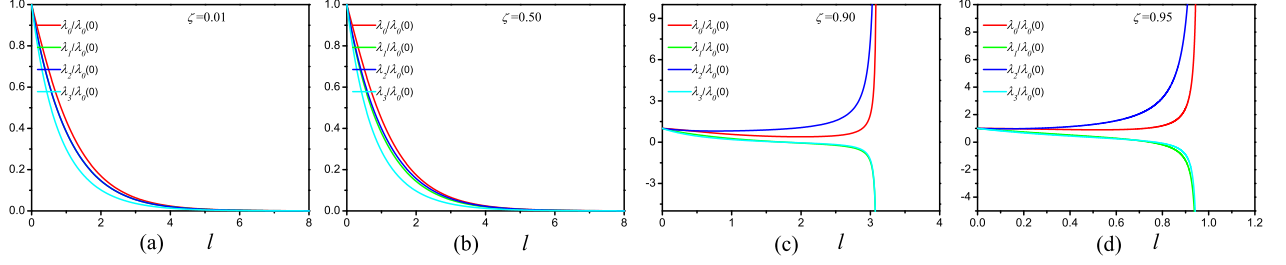


FIG. 1: (Color online) Energy-dependent evolutions of fermion-fermion strengths $\lambda_i(l)/\lambda_0(l=0)$ with distinct typical values of tilting parameter ζ and $\lambda_i(l=0) = 10^{-4}$ as well as $v_1 = v_2 = 10^{-2}$ (the basic results for $\lambda_i(0) < 0$ are similar and hence not shown here).

Before moving further, one also needs the rescaling transformations that are intimate bridges connecting two successive RG steps. To proceed, we can choose the $-ip_0$ term in the non-interacting action (1) as the fixed point following the spirit of standard RG approach [74], which is invariant under the whole RG process. As a consequence, one with the help of Eqs. (10) and (11) can straightforwardly derive the RG transformations for fields and other quantities [35, 36, 74, 78–80],

$$p_0 \rightarrow p'_0 = e^{-l} p_0, \quad (12)$$

$$E \rightarrow E' = e^{-l} E, \quad (13)$$

$$\theta \rightarrow \theta' = \theta, \quad (14)$$

$$\psi \rightarrow \psi' = e^{2l} \psi, \quad (15)$$

where the variable parameter l specifies an energy scale that is closely linked with the cutoff, namely $E = \Lambda e^{-l}$.

At this stage, we are in an appropriate situation to perform RG analysis. Concretely, we follow the strict procedures of RG approach [35, 74] and carry out tedious but straightforward calculations for all one-loop corrections provided in Appendix A. At first, it is worth pointing out that one-loop diagrams contributed by fermion-fermion interactions do not give rise to any corrections owing to conservations of momentum and energy. This indicates that free propagator cannot gain any corrections and hence fermion velocities and tilting parameter are invariant under RG analysis.

$$\frac{d\lambda_0}{dl} = -\lambda_0 + \frac{[\zeta^2 (\lambda_0^2 + \lambda_1^2 + \lambda_2^2 + \lambda_3^2 - 2\lambda_0\lambda_2) + 2(\zeta^* - 1)\lambda_0(\lambda_1 - \lambda_2)]}{2\pi v_1 v_2 \zeta^2 \zeta^*}, \quad (16)$$

$$\frac{d\lambda_1}{dl} = -\lambda_1 + \frac{2\zeta^2 [\lambda_1(2\lambda_0 + 2\lambda_1 - \lambda_2 - \lambda_3) - \lambda_0\lambda_3] + (\zeta^* - 1)[\lambda_0^2 + 5\lambda_1^2 + \lambda_2^2 + \lambda_3^2 + 2\lambda_1(\lambda_0 - \lambda_2 - \lambda_3) - 2\lambda_0\lambda_3]}{2\pi v_1 v_2 \zeta^2 \zeta^*}, \quad (17)$$

$$\frac{d\lambda_2}{dl} = -\lambda_2 + \frac{\{(1 - \zeta^*)[\lambda_0^2 + \lambda_1^2 + 5\lambda_2^2 + \lambda_3^2 + 2\lambda_2(\lambda_0 - \lambda_1 - \lambda_3) - 2\lambda_0\lambda_3] - \zeta^2 (\lambda_0^2 + \lambda_1^2 + \lambda_2^2 + \lambda_3^2 - 2\lambda_0\lambda_2)\}}{2\pi v_1 v_2 \zeta^2 \zeta^*}, \quad (18)$$

$$\frac{d\lambda_3}{dl} = -\lambda_3 + \frac{2\{\zeta^2 [(\lambda_1 + \lambda_2 - 2\lambda_3)\lambda_3 - \lambda_0\lambda_1] - (\zeta^* - 1)\lambda_0(\lambda_1 - \lambda_2)\}}{2\pi v_1 v_2 \zeta^2 \zeta^*}, \quad (19)$$

for type-I tilted Dirac fermions, and

$$\frac{d\lambda_0}{dl} = -\lambda_0 + \frac{2\zeta^* \lambda_0 \lambda_1}{\pi^2 \zeta |\zeta| v_1 v_2}, \quad (20)$$

$$\frac{d\lambda_1}{dl} = -\lambda_1 + \frac{\zeta^* (\lambda_0^2 + \lambda_1^2 + \lambda_2^2 + \lambda_3^2)}{2\pi^2 \zeta |\zeta| v_1 v_2}, \quad (21)$$

$$\frac{d\lambda_2}{dl} = -\lambda_2 + \frac{2\zeta^* [\lambda_0\lambda_3 - \lambda_2(\lambda_0 - \lambda_1 + 2\lambda_2 - \lambda_3)]}{\pi^2 \zeta |\zeta| v_1 v_2}, \quad (22)$$

$$\frac{d\lambda_3}{dl} = -\lambda_3 + \frac{2\zeta^* \lambda_0 \lambda_2}{\pi^2 \zeta |\zeta| v_1 v_2}. \quad (23)$$

for type-II tilted Dirac fermions. Two coefficients ζ^* and

ζ^* are designated as

$$\zeta^* \equiv \sqrt{1 - \zeta^2}, \quad \zeta^* \equiv 2|\zeta| - \sqrt{\zeta^2 - 1}, \quad (24)$$

to write above RG equations more compactly. We hereby would like to highlight that several approximations are exploited during the derivations of the RG equations for type-II tilted DSMs as provided in Appendix A. Next, we can extract the low-energy behaviors that are influenced or even dictated by the fermion-fermion interactions from above coupled RG evolutions of all interaction parameters.

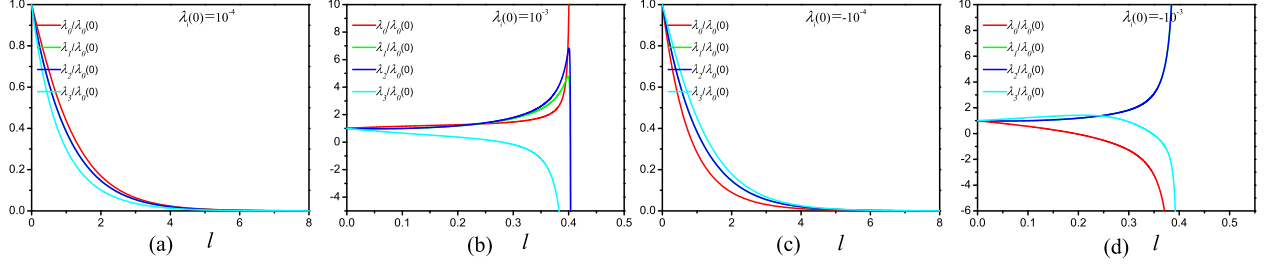


FIG. 2: (Color online) Energy-dependent evolutions of fermion-fermion strengths $\lambda_i(l)/\lambda_0(l=0)$ with distinct typical values of $\lambda_i(l=0)$ and tilting parameter $\zeta = 0.10$ as well as $v_1 = v_2 = 10^{-2}$.

IV. LOW-ENERGY FATES OF TYPE-I TILTED-DIRAC SEMIMETALS

To proceed, we are going to investigate the low-energy properties of tilted Dirac semimetals caused by the fermion-fermion interactions in the low-energy regime by virtue of their RG evolutions. Within this section, we endeavor to put our focus on the type-I tilted Dirac fermions and defer the type-II situation in the looming section.

In order to exactly capture the low-energy behaviors, one however is required to perform numerical analysis of RG equations (16)-(19) in that all interaction couplings are not independent but intimately entangled.

A. Roles of tilting parameter and starting values of fermion-fermion interactions

Learning from RG equations (16)-(19) for type-I tilted fermions (i.e., $|\zeta| < 1$), it is interesting to point out that the tilting parameter ζ always presents in the term of ζ^2 . As a result, one only needs to take into account either $\zeta > 0$ or $\zeta < 0$ as they share with the same coupled RG evolutions. In this respect, we hereafter consider the type-I tilted Dirac fermions with $\zeta > 0$. In addition, the tendencies of RG equations would be closely associated with the beginning values of fermion-fermion interactions. Without loss of generality, we assume all four types of fermion-fermion interactions to host an equivalent initial value dubbed $\lambda_i(0)$ with $i = 0, 1, 2, 3$. Moreover, the fermion velocities do not flow and hence can be regarded as certain constant (the basic results are insensitive to its specific value). To reiterate, both ζ and $\lambda_i(0)$ are crucial facets to determine the low-energy physics.

Therefore, it is of considerable significance to explore how these two parameters govern the low-energy physical behaviors of type-I tilted Dirac fermions. To proceed, we obtain several interesting results after carrying out the numerical analysis of entangled RG flows (16)-(19) and adopting several representative values for fermion velocities, tilting parameter, and $\lambda_i(0)$.

At first, we pick out an representative starting value of

fermionic interactions, such as $|\lambda_i(0)| = 10^{-4}$, which is insufficient large to induce any instabilities for un-tilted Dirac fermions (i.e., $\zeta = 0$). Learning from Fig. 1 with this fixed $|\lambda_i(0)|$ and distinct tilting parameters, we figure out that fermion-fermion couplings irrespective of repulsive or attractive interactions λ_i would gradually go towards Gaussian fixed point once the system is slightly tilted with a small ζ . However, while ζ is adequate large, fermion-fermion interactions can be driven to divergence at certain critical energy scale. These single out that some instability accompanied by potential phase transition can be expected in the low-energy regime [67, 70] as long as the Dirac system is sufficiently tilted. As a consequence, one can draw a conclusion that the type-I tilted Dirac system is more preferable to trigger instability compared to conventional Dirac fermions since the possibility of instability is of proportional relevance to the tilting parameter.

Subsequently, we take the tilting parameter as a fixed constant and inspect the role of starting values of fermion-fermion couplings in kindling possible instability. Specifically, choosing a typical value $\zeta = 0.1$ and performing analogous evaluations give rise to the key results delineated in Fig. 2. According to Fig. 2, we realize that the fermion-fermion couplings for type-I tilted Dirac fermions progressively climb down and are apparently attracted by the Gaussian fixed point (FP) once the beginning value $|\lambda_i(0)|$ is small. On the contrary, it is manifest that the Gaussian FP can be completely sabotaged and accordingly some instability would be activated by increasing the starting values of fermionic couplings. This implies that the initial values of fermion-fermion couplings, besides the tilting parameter ζ , are also very prone to produce the instability in the low-energy regime. It is worth stressing again that the basic results are insensitive to the signs of fermion-fermion interactions.

To be brief, both the tilting parameter ζ and fermionic starting value $\lambda_i(0)$ are helpful to the development of instability for the type-I tilted Dirac fermions in the low-energy regime. In addition, it is of particular interest to ask which of them takes a leading responsibility for pinpointing the low-energy states of type-I tilted Dirac fermions. To this end, we are going to concentrate on

this question in the next subsection.

B. Competition between tilting parameter and starting values of fermion-fermion interactions

In last subsection, we show that both tilting parameter ζ and initial values of fermion-fermion interactions $|\lambda_i(0)|$ are closely linked to potential instability. We hereby endeavor to explore how they compete and which of them is more favorable to spark certain instability in the type-I tilted Dirac fermions at the lowest-energy limit.

For type-I case, the tilting parameter ζ is restricted to $|\zeta| < 1$, whose concrete value principally dictates the structure of Dirac cones and low-energy excitations. In order to simplify the analysis, we divide the tilting parameter into three subregimes, namely Zone-I, Zone-II, and Zone-III, which correspond to $|\zeta| \rightarrow 0$, $|\zeta| \rightarrow 1$, and $|\zeta| \in \text{other values}$, respectively. At Zone-I, carrying out the similar procedures apparently indicates that the potential instabilities can only be produced once the initial fermion-fermion interactions are adequately large to exceed certain critical value regardless of repulsive or attractive interactions as displayed in Fig. 3. Clearly, these results are in well agreement with untilted Dirac fermions in that tilted Dirac fermions naturally reduce to conventional Dirac fermions at $\zeta \rightarrow 0$ and hence the potential instability can only be generated once the initial fermion-fermion interactions exceed certain critical value [75–77].

Afterwards, we move to Zone-III. Following the related steps, the tilted Dirac fermions at this regime unambiguously exhibit analogous low-energy behaviors to their counterparts in Zone-I owing to similar Fermi surfaces and Dirac cones. A slight distinction between these two situations is that the critical value of fermion-fermion interaction, beyond which the instability is triggered, would be progressively decreased while the tilting parameter ζ is tuned up. With these respects, the instability can be inescapably induced by a sufficiently large $|\lambda_i(0)|$ no matter what a specific value of ζ is assigned. Accordingly, the initial values of fermion-fermion couplings $|\lambda_i(0)|$ are more significant than the tilting parameter ζ at both Zone-I and Zone-III. In sharp distinction to Zone-I and Zone-III, as demonstrated in Fig 4, the type-I tilted Dirac fermion can be driven into certain instability by a small fermion-fermion interaction that is much smaller than critical value $|\lambda_i(0)|$ while the Zone-II is approached. In other words, an underlying instability generally sets in if the Lifshitz phase point ($|\zeta| = 1$) [81–84], which separates type-I and type-II tilted Dirac fermions [35, 36], is accessed even though the starting values of fermion-fermion strengths are very small. One therefore naturally expects the topological changes of Fermi surfaces may be responsible for this unique phenomenon. In this regard, one may ascribe this consequence to the singular effects caused by the very Lifshitz phase point [35]. At this stage, one can deduce that the tilting parameter ζ is

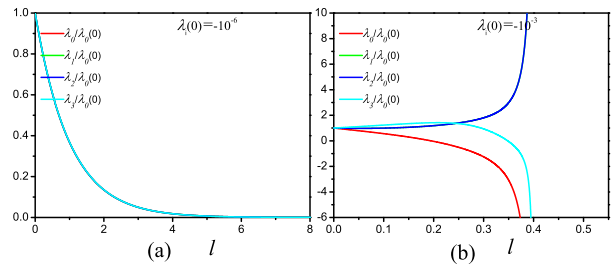


FIG. 3: (Color online) Energy-dependent evolutions of fermion-fermion strengths $\lambda_i(l)/\lambda_0(l=0)$ for (a) $\lambda_i(0) = -10^{-6}$ and (b) $\lambda_i(0) = -10^{-3}$ at tilting parameter $\zeta \rightarrow 0$ and $v_1 = v_2 = 10^{-2}$ (the basic results for $\lambda_i(0) > 0$ are similar and hence not shown here).

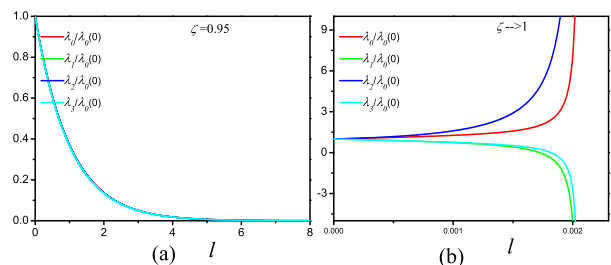


FIG. 4: (Color online) Energy-dependent evolutions of fermion-fermion strengths $\lambda_i(l)/\lambda_0(l=0)$ for (a) $\zeta = 0.95$ and (b) $\zeta \rightarrow 1$ at $\lambda_i(0) = 10^{-6}$ and $v_1 = v_2 = 10^{-2}$ (the principal conclusions for $\lambda_i(0) < 0$ are analogous and hence not shown here).

more important at Zone-II as ζ is directly associated with the Fermi surface's structure of tilted Dirac fermions.

To reiterate, either the increase of starting values of fermion-fermion strengths $|\lambda_i(0)|$ or tilting parameter ζ for type-I tilted Dirac fermions is helpful to develop certain instability in the low-energy regime. In particular, $|\lambda_i(0)|$ and ζ play a more crucial role in igniting the potential instability at Zone-I (or Zone-III) and Zone-II, respectively. Fig. 5(a) and Table I briefly summarize our primary conclusions.

V. LOW-ENERGY FATES OF TYPE-II TILTED-DIRAC SEMIMETALS

Within this section, we dwell on the physical properties of type-II tilted Dirac fermions caused by fermion-fermion interactions in the low-energy. Hereby, we focus on the $\zeta > 0$ case at first and then present our discussions for the $\zeta < 0$ situation at the end of this section.

A. Roles of tilting parameter and starting values of fermion-fermion interactions

In order to capture the effects of $|\lambda_i(0)|$ and ζ on the type-II system, we follow the procedures in previous section, namely taking $|\lambda_i(0)|$ as a fixed value and adjusting the values of ζ to observe the impact induced by ζ and vice versa. Without loss of generality, we choose $|\lambda_i(0)| = 10^{-3}$ and show the results in Fig. 6 with variation of ζ . In the light of these, we figure out that the potential instability triggered at a small ζ would be destroyed and replaced by the Gaussian FP as the tilting parameter is increased. In apparent distinction to type-I case, this signals that the increase of ζ brings detriments to the emergence of instability for type-II tilted Dirac fermions. Despite the basic conclusions are robust irrespective of signs of $\lambda_i(0)$, there are different divergence trends for $\lambda_i(0) > 0$ and $\lambda_i(0) < 0$, which will be studied in Sec. VI.

In addition, we consider the tilting parameter as a constant, for instance $\zeta = 5$, adjust the starting values of fermion-fermion couplings, and plot the numerical results in Fig. 7 after performing numerical analysis of coupled RG equations (20)-(23). Fig. 7 unambiguously delivers that trajectories of λ_i can be converted from Gaussian FP to instability via tuning up the value of $|\lambda_0(0)|$. This implies that there always exists a critical value $|\lambda_i^c(0)|$, beyond which certain instability is conventionally expected. It indicates that the increase of initial values of fermion-fermion interactions is in favor of the generation of instability in the type-II tilted fermionic system. This conclusion is well in line with the type-I case.

To reiterate, we find that the effects of two parameters $|\lambda_i(0)|$ and ζ on the type-II Dirac fermions are opposite. Specifically, the increase of $|\lambda_i(0)|$ prefers to switch on the instability in the low-energy. Rather, tuning up ζ is harmful to the development of instability.

B. Competition between tilting parameter and starting values of fermion-fermion interactions

In last subsection, we deliver that the initial values of fermion-fermion couplings $|\lambda_i(0)|$ and tilting parameter ζ in principle promote and suppress the instability of the type-II tilted Dirac fermions, respectively. At this stage, it is now tempting to inquire which of these two parameters plays a leading role in dictating low-energy states within certain parameter-space region. Motivated by this, we hereby are going to response this question. For convenience, the tilting parameter ζ is at first assumed to be positive.

To proceed, the tilting parameter ζ , in analogous to Type-I case, can also cluster into three sets, namely Zone – I with $|\zeta| \rightarrow 1$, Zone – II with $|\zeta| \rightarrow \infty$, and Zone – III with $|\zeta| \in \text{other values}$, respectively. At $\zeta \rightarrow \text{Zone – I}$, each of the coupled RG equations (20)-

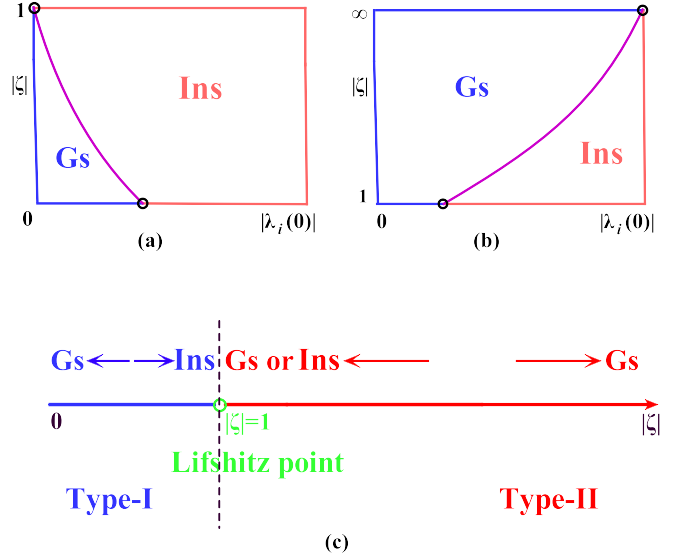


FIG. 5: (Color online) Schematic phase diagrams in the $\zeta - \lambda_i(0)$ plane for (a) type-I and (b) type-II tilted Dirac semimetals. Subfigure (c) summarizes both (a) and (b) by schematically displaying the key points separated by the Lifshitz phase point. For convenience, “Gs” and “Ins” are exploited to serve as Gaussian FP and certain instability, respectively (The dominant phases induced by these instabilities are carefully examined in Sec. VIB and schematically exhibited in Fig. 14).

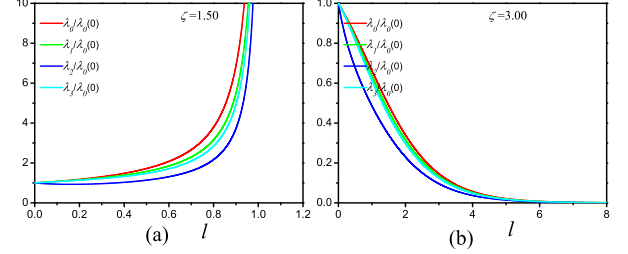


FIG. 6: (Color online) Energy-dependent evolutions of fermion-fermion strengths $\lambda_i(l)/\lambda_0(l=0)$ for (a) $\zeta = 1.5$ and (b) $\zeta = 3.0$ at $\lambda_i(0) = 10^{-3}$ and $v_1 = v_2 = 10^{-2}$ (the basic results for $\lambda_i(0) < 0$ are similar and the tendency of divergences are analogous to Fig. 7. Hence they are not shown here).

(23) can be formally rewritten as $d\lambda = \lambda(1 - c\lambda)$ with c being a finite constant and $1/c$ the critical value $\lambda^c(0)$ that is the minimum value to generate an instability. In other words, λ is only increased once $\lambda(0)$ exceeds $1/c$ with $\lambda(0) > 0$. Accordingly, in a sharp contrast to type-I case where an instability is always produced at $\zeta \rightarrow 1$, we realize that ζ is no longer the key factor to trigger an instability at Zone – I. Rather, $|\lambda_i(0)|$ solely pins down whether certain instability can be induced. To be specific, an instability sets in once $|\lambda_i(0)|$ is large enough to go beyond some critical value. Otherwise, the system directly evolves to Gaussian FP. Fig 8(a) and (b) clearly

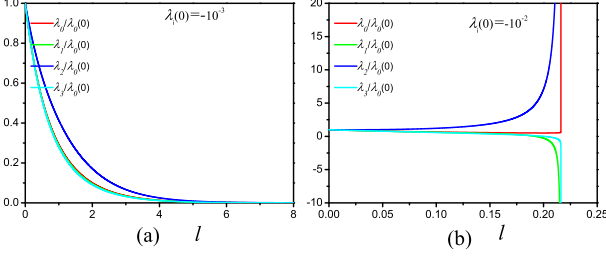


FIG. 7: (Color online) Energy-dependent evolutions of fermion-fermion strengths $\lambda_i(l)/\lambda_0(l=0)$ for (a) $\lambda_i(0) = -10^{-3}$ and (b) $\lambda_i(0) = -10^{-2}$ at tilting parameter $\zeta = 5$ and $v_1 = v_2 = 10^{-2}$ (the basic results for $\lambda_i(0) > 0$ are similar and the tendency of divergences are analogous to Fig. 6. Hence they are not shown here).

illustrate the behaviors approaching the Zone – I. Consequently, we would like to stress that the qualitative results are insusceptible to the concrete values of $|\lambda_i(0)|$. As is analogous to type-I situation, one can infer that the basic conclusions are well consistent with Zone – I's when the tilting parameter ζ belongs to Zone – III. However, a bigger $|\lambda_i(0)|$ is required to activate a potential instability in that ζ prefers to hinder the development of instability as pointed out in Sec. V A. Further, we move to Zone – II of type-II case. Implementing and practicing aforementioned strategies when ζ approaches Zone – II, one can examine and realize that the threshold of fermion-fermion couplings goes towards infinity, i.e., $|\lambda_i^c(0)| \rightarrow \infty$. As a consequence, the type-II tilted fermion inescapably flows towards the Gaussian FP at the lowest-energy limit. The numerical evaluations of coupled RG equations corroborate these analysis as depicted in Fig. 8(c). Learning from Fig. 8, we can also find that the underlying instability can be switched off once the tilting parameter ζ is increased. Given that fermion-fermion interactions cannot be taken too strong, the Gaussian FP would be always expected as long as ζ is sufficient large. In a word, the low-energy fates of the type-II tilted Dirac fermions are firmly rooted in the considerable competition between $|\lambda_i(0)|$ and ζ . The tilting parameter ζ becomes a major ingredient that is able to be responsible for the low-energy states as long as it is sufficiently large or restricted to Zone – II. This signals that any instabilities are not allowed in the low-energy regime. However, $|\lambda_i(0)|$ dominates over the tilting parameter in case ζ is small or accessing Zone – I.

Before closing this section, we finally address several comments on the $\zeta < 0$ situation. In apparent variance with type-I case at which the coupled RG evolutions keep invariant under the transformation $\zeta \rightarrow -\zeta$, it is henceforth worth highlighting that the tilting parameter ζ in the coupled RG equations (20)-(23) can appear in terms of either ζ , $|\zeta|$, or ζ^2 . At the first sight, this signals that we need to study $\zeta > 0$ and $\zeta < 0$ separately. However, after revisiting the coupled RG evolutions of type-II tilted Dirac fermions in more details, it is interesting to point

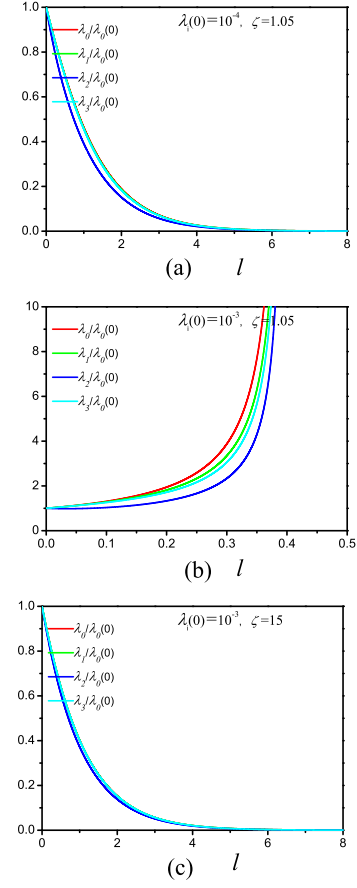


FIG. 8: (Color online) Energy-dependent evolutions of fermion-fermion strengths $\lambda_i(l)/\lambda_0(l=0)$ for (a) $\lambda_i(0) = 10^{-4}$, $\zeta = 1.05$; (b) $\lambda_i(0) = 10^{-3}$, $\zeta = 1.05$; and (c) $\lambda_i(0) = 10^{-3}$, $\zeta = 15$ at $v_1 = v_2 = 10^{-2}$ (the basic results for $\lambda_i(0) < 0$ are similar and the tendency of divergences are analogous to Fig. 7. Hence they are not shown here).

out that the RG equations for $\zeta > 0$ with $\lambda_i(0) > 0$ and $\lambda_i(0) < 0$ exactly correspond to their $\zeta < 0$ counterparts with $\lambda_i(0) < 0$ and $\lambda_i(0) > 0$, respectively. In this sense, it is sufficient to investigate $\zeta > 0$ case as the results for $\zeta < 0$ can be easily obtained via replacing $\lambda > 0$ with $\lambda < 0$. In short, our primary conclusions for type-II tilted Dirac fermions are schematically displayed and vigilantly collected by Fig. 5(b) and Table II.

VI. INSTABILITIES AND DOMINANT PHASES

On the basis of previous analysis, several potential instabilities can be generated for both type-I and type-II tilted Dirac semimetals attesting to the competitions among distinct sorts of fermion-fermion interactions in the low-energy regime. Gathering all principal results presented in Sec. IV and Sec. V, we figure out that the potential instabilities are broken into several distinguished sorts with variations of the tilting parameter and start-

TABLE I: Low-energy fates of type-I tilted Dirac fermions with variations of tilting parameter ζ and beginning values of fermion-fermion couplings $\lambda_i(0)$. To be convenient, “Gs” and “Ins” stand for Gaussian FP and certain instability, respectively. In addition, we have already introduced Zone – I, Zone – II, and Zone – III in Sec. IV B to classify values of ζ for type-I tilted DSMs. Moreover, Ins-I, Ins-II, Ins-III, and Ins-IV designating distinct types of instabilities and the leading phases around these instabilities are carefully investigated in Sec. VI and schematically displayed in Fig. 14.

	$ \lambda_i(0) $	ζ		
		Zone – I	Zone – III	Zone – II
$\lambda_i(0) > 0$	Small	Gs	Gs	Ins-I
	Medium	Gs	Ins-I	Ins-I
	Large	Ins-IV	Ins-III	Ins-I
$\lambda_i(0) < 0$	Small	Gs	Gs	Ins-II
	Medium	Gs	Gs	Ins-II
	Large	Ins-II	Ins-II	Ins-II

ing values of fermion-fermion interactions. Subsequently, we endeavor to classify these underlying instabilities and then determine the dominant phases around them one by one.

A. Classifications of instabilities

At first, we consider type-I tilted Dirac fermions. On one side, Fig. 9(a) clearly exhibits an instability with $\lambda_i(0) > 0$. In this case, both fermion-fermion couplings λ_0 and λ_2 go up monotonously and diverge at critical energy scale without sign change. In comparison, λ_1 and λ_3 gradually increase but quickly decrease, change signs and eventually flow infinity in close proximity to the critical energy scale. To be convenient, we designate this kind of instability as the first case of instability (Ins-I). On the other side, one can obviously realize that the instability illustrated in Fig. 9(b) features qualitative differences of evolutions compared to its Ins-I counterpart. Specifically, both λ_1 and λ_2 flow towards the strong couplings without sign change at the critical energy scale. However, the divergences of λ_0 and λ_3 at the critical energy scale are accompanied with sign changes. Analogously, this kind of instability is denominated as the second class of instability (Ins-II). What is more, there exists a unique kind of instability as demonstrated apparently in Fig 9(c), which is of remarkable distinction from both Ins-I and Ins-II. To be concrete, the fermion-fermion coupling λ_0 quickly increases with lowering the energy scale and directly tends to diverge at some critical point. In contrast, both λ_1 and λ_2 progressively climb up and then diverge abruptly in the opposite direction near the critical point. However, the interaction parameter λ_3 is monotonously decreased until diverges negatively in the proximity of the critical point. In other words, there is only one fermion-fermion

interaction that diverges positively and all the others negatively. In order to distinguish this instability from Ins-I and Ins-II, we thereby nominate it as the third class of instability (Ins-III) to specify these particular low-energy behaviors of fermion-fermion couplings. What is more, there exists another class of instability as illustrated in Fig. 9(d). In this circumstance, both fermion-fermion strengths λ_0 and λ_1 are monotonically and rapidly increased but instead λ_2 and λ_3 are drastically pulled down with the energy scales lowering. At last, all of them flow towards the strong couplings at a critical point. Analogously, we consider this kind of instability as the fourth class of instability (Ins-IV).

Next, we move to the type-II tilted Dirac fermions. At $\lambda_i(0) < 0$, we find the possible instability in type-II tilted system corresponds to Ins-I. In comparison, another type of instability, namely Ins-II, is developed at $\lambda_i(0) > 0$. Other than Ins-I, Ins-II, Ins-III, and Ins-IV, Fig. 9(e) is unambiguously indicative of an outlandish instability. In this circumstance, all the energy-dependent trajectories of $\lambda_i/\lambda_0(0)$ prefer to gradually increase and diverge in the same direction without any sign change. Given that these behaviors of fermion-fermion couplings are distinct from all the other four sorts of instabilities, the fifth class of instability (Ins-V) is employed to characterize this kind of unique phenomenon. Conventionally, instabilities of fermion-fermion interactions in the low-energy correspond to the relatively fixed pints (RFPs) [67, 70, 71], at which phase transitions are usually accompanied. In order to capture more information of these instabilities, it is therefore interesting to judge whether tilted Dirac fermions possess any RFPs of fermion-fermion couplings at the lowest-energy limit. To this end, we can measure all four-fermion interaction parameters with one of them whose sign is unchanged during the RG process [67, 70]. For instance, we pick out λ_0 to examine whether the tilted Dirac fermion hosts any RFPs in the parameter space, which are described by the evolutions of λ_i/λ_0 . To proceed, we derive and plot the trajectories of λ_i/λ_0 (or λ_i/λ_2) approaching the corresponding RFPs (possible instabilities) upon lowering the energy scale as clearly characterized in Fig. 9(f)-(j). These results manifestly show the distinctions among different classes of instabilities. With the help of these RFPs, it would be very helpful to investigate the physical implications on the tendency of strong couplings for the fermion-fermion interactions [67, 70, 71].

To be brief, the five distinct classes of instabilities, namely Ins-I, Ins-II, Ins-III, Ins-IV, and Ins-V, can be activated attesting to the intimate interplays among four kinds of fermion-fermion interactions in tandem with the tilting parameter in the low-energy regime of tilted Dirac semimetals. Specifically, Ins-I, Ins-II, Ins-III, and Ins-IV are expected in the type-I tilted system. Rather, the type-II tilted Dirac fermions host Ins-I and Ins-V. Table I together with Table II as well as Fig. 5 present the full information of all five sorts of instabilities and schematically exhibit physical pictures of both type-I and type-II

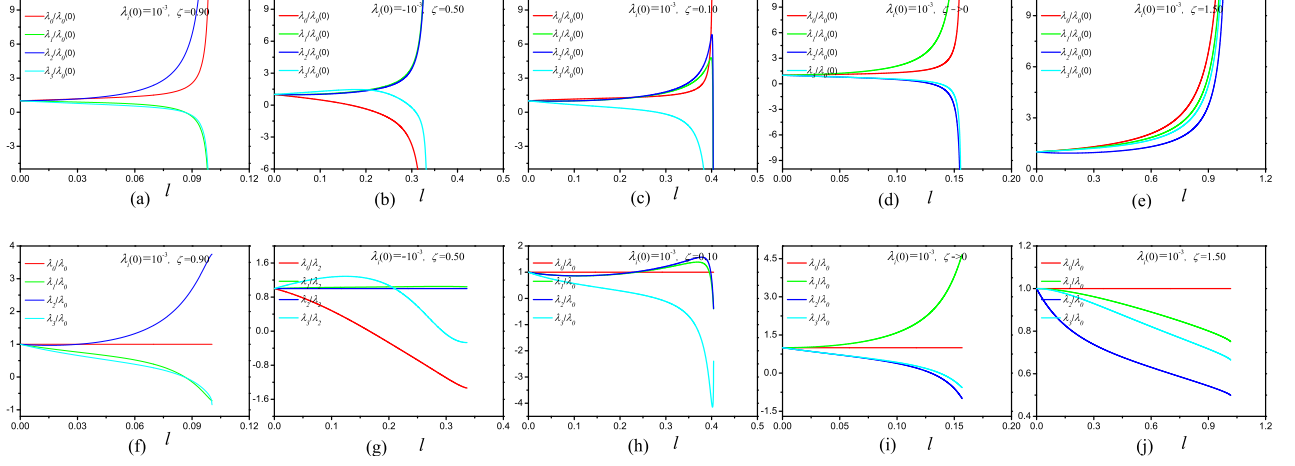


FIG. 9: (Color online) Potential five distinct types of instabilities for (a) Ins-I (with $\lambda_i(0) = 10^{-3}$ and $\zeta = 0.9$); (b) Ins-II (with $\lambda_i(0) = -10^{-3}$ and $\zeta = 0.5$); (c) Ins-III (with $\lambda_i(0) = 10^{-3}$ and $\zeta = 0.1$); (d) Ins-IV (with $\lambda_i(0) = 10^{-3}$ and $\zeta \rightarrow 0$); and (e) Ins-V (with $\lambda_i(0) = 10^{-3}$ and $\zeta = 1.5$) at $v_1 = v_2 = 10^{-2}$, whose RFPs correspond to subfigures (f), (g), (h), (i) and (j), respectively.

TABLE II: Low-energy fates of type-II tilted Dirac fermions with variations of tilting parameter ζ and beginning values of fermion-fermion couplings $\lambda_i(0)$. Hereby, “Gs” and “Ins” are again adopted to characterize Gaussian FP and certain instability, respectively. In addition, Ins-I, Ins-V specify distinct types of instabilities, which are addressed and denominated in Sec. VI. Further, Zone – I, Zone – II, and Zone – III are designated in Sec. VB to discriminate values of ζ for type-II tilted DSMs (In Sec. VIB, the leading phases generated by Ins-I and Ins-V are carefully investigated and schematically displayed in Fig. 14).

	$ \lambda_i(0) $	ζ		
		Zone – I	Zone – III	Zone – II
$\lambda_i(0) > 0$	Small	Gs	Gs	Gs
	Medium	Ins-V	Gs	Gs
	Large	Ins-V	Ins-V	Gs
$\lambda_i(0) < 0$	Small	Gs	Gs	Gs
	Medium	Ins-I	Gs	Gs
	Large	Ins-I	Ins-I	Gs

tilted Dirac fermions.

B. Dominant phases

To proceed, we endeavor to determine the potential leading phases in the vicinity of these distinct types of instabilities. For this purpose, we add the following source terms into the effective action (5) [67, 85, 86]

$$S_{\text{source}} = \int d\tau \int d^2\mathbf{x} \sum_i \Delta_i \psi^\dagger \mathcal{G}_i \psi, \quad (25)$$

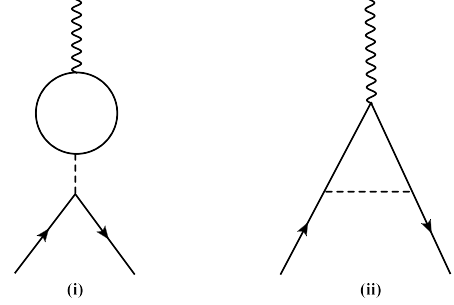


FIG. 10: One-loop corrections to the bilinear fermion-source terms. The solid, dash, and wave lines serve as the fermion, fermion-fermion interaction and source term field, respectively.

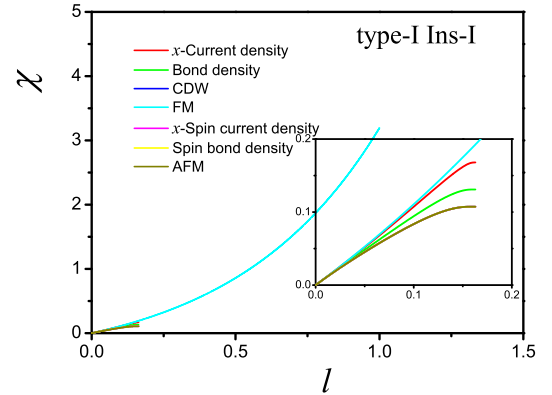


FIG. 11: (Color online) Susceptibilities approaching the Ins-I for type-I tilted DSMs. The inset shows the flows of beginning regime (the basic results for the Ins-IV are similar to Ins-I and hence are not shown).

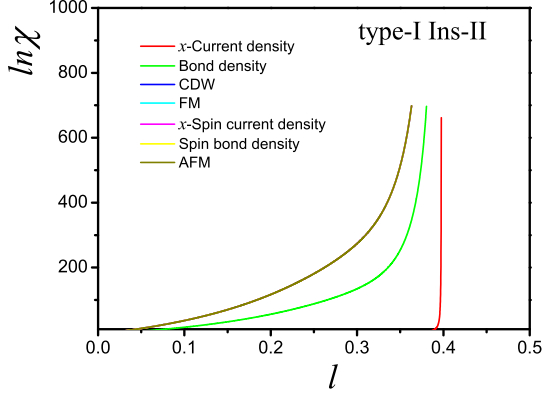


FIG. 12: (Color online) Susceptibilities approaching the Ins-II for type-I tilted DSMs. The inset shows the flows of beginning regime (The basic results for the Ins-III are similar to Ins-II and hence are not shown).

where the matrix \mathcal{G}_i defines the various fermion bilinears and Δ_i refers to the strength of corresponding fermion-source term. The susceptibility of potential phase is closely related to Δ_i according to [67, 70]

$$\delta\chi_i = -\frac{\partial^2 \delta f}{\partial \Delta_i(0) \partial \Delta^*(0)}, \quad (26)$$

with f being the free energy density. To be specific, the matrices $\mathcal{G}_1 = \sigma_1$, $\mathcal{G}_2 = \sigma_2$, $\mathcal{G}_3 = \sigma_3$, $\mathcal{G}_4 = \tau_k \otimes \sigma_0$ (τ_k with $k = 1, 2, 3$ acts on the spin space), $\mathcal{G}_5 = \tau_k \otimes \sigma_1$, $\mathcal{G}_6 = \tau_k \otimes \sigma_2$, and $\mathcal{G}_7 = \tau_k \otimes \sigma_3$ correspond to x -current density, bond density, charge density wave, ferromagnet, x -spin current density, spin bond density, and antiferromagnet, respectively [13, 86]. Here, it is necessary to point out that the x -current and x -spin current density would break certain symmetry. However, these conversed symmetry currents cannot be regarded as some true order parameters. For completeness, we also list them as potential stable states. In addition, the bond density and spin bond density are associated with spin-independence anisotropic and spin-dependence anisotropic modulations of the nearest-neighbor hopping amplitude [13].

Subsequently, we move our focus to one-loop corrections to the source terms shown in Fig. 10. After performing long but straightforward calculations [13, 67, 70, 86] and employing the RG scalings (12)-(15), we obtain the energy-dependent source terms,

$$\frac{d\Delta_1}{dl} = \left[1 + \frac{(\lambda_0 - \lambda_1 - \lambda_2 - \lambda_3)(1 - \zeta^*)}{2\pi v_1 v_2 \zeta^2} \right] \Delta_1, \quad (27)$$

$$\frac{d\Delta_2}{dl} = \left[1 + \frac{(\lambda_0 - \lambda_1 - \lambda_2 - \lambda_3)(1 - \zeta^*)}{2\pi \zeta^2 \zeta^* v_1 v_2} \right] \Delta_2, \quad (28)$$

$$\frac{d\Delta_3}{dl} = \left[1 + \frac{(\lambda_0 - \lambda_1 - \lambda_2 - \lambda_3)}{2\pi v_1 v_2 \zeta^*} \right] \Delta_3, \quad (29)$$

$$\frac{d\Delta_4}{dl} = \Delta_4, \quad (30)$$

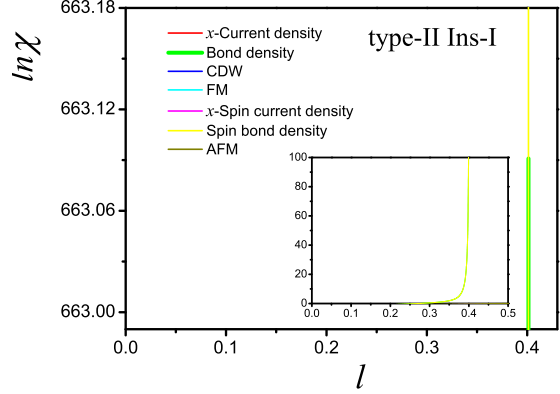


FIG. 13: (Color online) Susceptibilities approaching the Ins-I for type-II tilted DSMs. The inset shows the flows of full regime.

$$\frac{d\Delta_5}{dl} = \left[1 + \frac{(3\lambda_0 + \lambda_1 - 3\lambda_2 - 3\lambda_3)(1 - \zeta^*)}{3\pi v_1 v_2 \zeta^2} \right] \Delta_5, \quad (31)$$

$$\frac{d\Delta_6}{dl} = \left[1 + \frac{(3\lambda_0 - 3\lambda_1 + \lambda_2 - 3\lambda_3)(1 - \zeta^*)}{3\pi v_1 v_2 \zeta^2 \zeta^*} \right] \Delta_6, \quad (32)$$

$$\frac{d\Delta_7}{dl} = \left[1 + \frac{(3\lambda_0 - 3\lambda_1 - 3\lambda_2 + \lambda_3)}{3\pi v_1 v_2 \zeta^*} \right] \Delta_7. \quad (33)$$

for type-I tilted DSMs, and

$$\frac{d\Delta_j}{dl} = \Delta_j \quad \text{with } j = 1, 3 - 5, 7, \quad (34)$$

$$\frac{d\Delta_2}{dl} = \left[1 + \frac{\zeta^*(\lambda_2 - \lambda_0 + \lambda_1 + \lambda_3)}{\pi^2 \zeta |\zeta| v_1 v_2} \right] \Delta_3, \quad (35)$$

$$\frac{d\Delta_6}{dl} = \left[1 - \frac{2\zeta^*(3\lambda_0 - 3\lambda_1 + \lambda_2 - 3\lambda_3)}{3\pi^2 \zeta |\zeta| v_1 v_2} \right] \Delta_7, \quad (36)$$

for type-II case. Here ζ^* and ζ^* are denominated in Eq. (24).

Generally, the dominant phase nearby an instability is accompanied by the leading susceptibility [13, 67, 86–88]. Accordingly, we are suggested to evaluate the susceptibilities of all these eight potential phases approaching the five different instabilities and sort out the dominant one. To this end, we need to combine the RG flow equations of interaction parameters in Eqs. (16)-(23) and energy-dependent evolutions of source terms (30)-(36) as well as the relationships between susceptibilities and source terms (26). The primary results are presented in Figs. 11, 12 and 13 after carrying out the numerical analysis.

At first, we consider type-I tilted DSMs at which Ins-I, Ins-II, Ins-III, and Ins-IV can be induced. All eight types of susceptibilities are increased while the Ins-I is accessed. In particular, the ferromagnet(FM) gets the largest susceptibility as clearly depicted in Fig. 11. Although the susceptibility is not divergent, we would like to expect that these two phases are more preferable than others around the Ins-I. Once the system approaches the Ins-II, Fig. 12 manifestly exhibits that the antiferromagnet

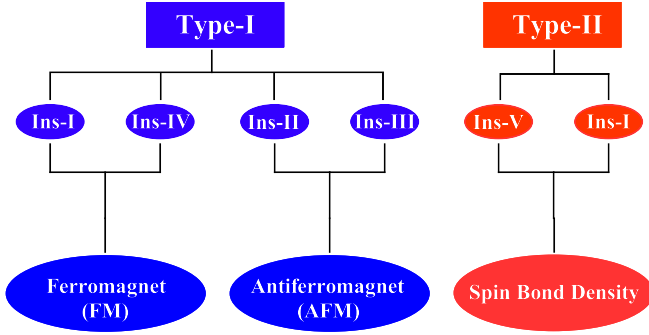


FIG. 14: (Color online) Schematic diagrams sketching the leading phases accompanied by distinct sorts of instabilities for both type-I and type-II tilted DSMs. The details of instabilities including Ins-I to Ins-V are presented in Table I, Table II and Fig. 5.

(AFM) susceptibility climbs up very quickly and firstly goes towards infinity. This apparently signals that the AFM is the dominant phase among all eight potential candidates in proximity to the Ins-II. It is therefore interesting to point out that the leading phase around Ins-II is roughly consistent with the one caused by Coulomb interaction in the untilted DSMs [69]. Performing the similar steps, we find that the basic results for approaching Ins-III and Ins-IV are qualitatively consistent with their Ins-II and Ins-I counterparts. Next, we move to the type-II case at which only Ins-I and Ins-V are allowed to be triggered. Learning from Fig. 13, we can reach that the spin bond density is the most competitive one among all possible phases in the vicinity of Ins-I for type-II tilted DSMs. In addition, we address that the Ins-V shares the similar conclusion with Ins-I. To be brief, we conclude that FM, AFM, and spin bond density are more preferable as the instabilities are approached. Concretely, which of them is the leading one would heavily rely upon the tilting parameter and concrete types of instabilities.

VII. SUMMARY

In summary, we investigate the low-energy states of both type-I and type-II tilted DSMs in the presence of four distinct types of fermion-fermion interactions. By virtue of the powerful RG approach [74], we derive the energy-dependent coupled flow equations of all interaction parameters. Carrying out detailed analysis of these evolutions signals that the effects of fermionic interaction on low-energy behaviors of tilted DSMs heavily hinge upon the tilting parameter ζ and initial value of fermion-fermion interaction $\lambda_i(0)$. Several interesting low-energy properties of tilted DSMs are manifestly delivered.

Concretely, we find the tilted DSMs with lowering the energy scale can either tend to the Gaussian FP or exhibit

an instability that is linked to certain phase transition. At the outset, we realize that the parameters ζ and $\lambda_i(0)$ play different roles in pinning down the low-energy fates of type-I and type-II tilted DSMs. For type-I tilted DSMs, either increase of ζ or $\lambda_i(0)$ would be profitable to trigger an instability in the low-energy regime. In a contrast, tuning up the initial value of the four-fermion interaction is still favorable to the generation of instability for type-II tilted DSMs. However, the tilting parameter ζ is not proportional to the instability. This implies that the system unavoidably flows towards the Gaussian FP once the ζ is sufficiently large. In addition, we figure out the parameters ζ and $\lambda_i(0)$ strongly compete within distinct zones of ζ . In the type-I tilted DSMs, $\lambda_i(0)$ wins the competition at both Zone-I ($\zeta \rightarrow 0$) and Zone-II ($\zeta \rightarrow 1$). Whereas the tilting parameter ζ plays a more crucial role in igniting the potential instability at Zone-III characterized by $\zeta \in \text{other values}$. In comparison, the parameter $|\lambda_i(0)|$ dominates over the tilting parameter if ζ is small for type-II tilted DSMs. Once ζ is large, it becomes a leading facet to determine the low-energy state. In particular, any instability is not allowed at $\zeta \rightarrow \infty$. Moreover, all of underlying instabilities induced by the fermion-fermion interactions via appropriately adjusting the two parameters ζ and $\lambda_i(0)$ can be clustered into five distinct classes, which own qualitatively different energy-dependent trajectories and RFPs at the critical energy scale and are nominated as Ins-I, Ins-II, Ins-III, Ins-IV, and Ins-V, respectively. The detailed information is provided in Table I, Table II and Fig. 9. Based on our studies, Ins-I, Ins-II, Ins-III, and Ins-IV can be expected in the type-I tilted DSMs. Rather, the type-II tilted Dirac fermions only host Ins-I and Ins-V. After computing and comparing susceptibilities of eight potential phases around these instabilities, we find that the dominant phases are closely related to the tilting parameter and concrete instabilities. To be brief, the type-I and the type-II tilted Dirac fermions exhibit distinct low-energy physical behaviors under the effects of fermion-fermion interactions.

In principle, all of these interesting physical behaviors for type-I and type-II tilted DSMs caused by the four-fermion interactions in the low-energy regime would be remarkably instructive to further study the physical properties affected by instabilities, detect the positions of potential phase transitions and so on in the tilted DSMs or other tilted systems. In a word, we expect our efforts can play an important positive role in both future theoretical and experimental explores in tilted fermionic systems.

ACKNOWLEDGEMENTS

J.W. is partially supported by the National Natural Science Foundation of China under Grant 11504360.

AUTHOR CONTRIBUTION STATEMENTS

J. W. initiated and supervised the project as well as performed the numerical analysis and wrote the manuscript. J.Q.L. carried out the analytical calculations. Z.D.X. participated in some discussions and provided several useful suggestions.

Appendix A: One-loop corrections

After carrying out long but straightforward one-loop calculations [67, 70, 71] and collecting all corrections, we are left with the following results,

$$S_{\xi}^{\lambda_0} = \int \frac{dp'_0 dp''_0 dp'''_0}{(2\pi)^3} \frac{d^2 \mathbf{p}' d^2 \mathbf{p}'' d^2 \mathbf{p}'''}{(2\pi)^6} [\psi_{\xi\alpha}^\dagger(p'_0, \mathbf{p}') \sigma_0 \psi_{\xi\alpha}(p''_0, \mathbf{p}'') \psi_{\xi'\alpha'}^\dagger(p'''_0, \mathbf{p}''') \sigma_0 \psi_{\xi'\alpha'}(p'_0 + p''_0 - p'''_0, \mathbf{p}' + \mathbf{p}'' - \mathbf{p}''')] \times \frac{[\zeta^2 (\lambda_0^2 + \lambda_1^2 + \lambda_2^2 + \lambda_3^2 - 2\lambda_0\lambda_2) + 2(\zeta^* - 1)\lambda_0(\lambda_1 - \lambda_2)] l}{2\pi v_1 v_2 \zeta^2 \zeta^*}, \quad (\text{A1})$$

$$S_{\xi}^{\lambda_1} = \int \frac{dp'_0 dp''_0 dp'''_0}{(2\pi)^3} \frac{d^2 \mathbf{p}' d^2 \mathbf{p}'' d^2 \mathbf{p}'''}{(2\pi)^6} [\psi_{\xi\alpha}^\dagger(p'_0, \mathbf{p}') \sigma_1 \psi_{\xi\alpha}(p''_0, \mathbf{p}'') \psi_{\xi'\alpha'}^\dagger(p'''_0, \mathbf{p}''') \sigma_1 \psi_{\xi'\alpha'}(p'_0 + p''_0 - p'''_0, \mathbf{p}' + \mathbf{p}'' - \mathbf{p}''')] \times \frac{(\zeta^* - 1) [\lambda_0^2 + 5\lambda_1^2 + \lambda_2^2 + \lambda_3^2 + 2\lambda_1(\lambda_0 - \lambda_2 - \lambda_3) - 2\lambda_0\lambda_3] + 2\zeta^2 [\lambda_1(2\lambda_0 + 2\lambda_1 - \lambda_2 - \lambda_3) - \lambda_0\lambda_3]}{2\pi v_1 v_2 \zeta^2 \zeta^*} l, \quad (\text{A2})$$

$$S_{\xi}^{\lambda_2} = - \int \frac{dp'_0 dp''_0 dp'''_0}{(2\pi)^3} \frac{d^2 \mathbf{p}' d^2 \mathbf{p}'' d^2 \mathbf{p}'''}{(2\pi)^6} [\psi_{\xi\alpha}^\dagger(p'_0, \mathbf{p}') \sigma_2 \psi_{\xi\alpha}(p''_0, \mathbf{p}'') \psi_{\xi'\alpha'}^\dagger(p'''_0, \mathbf{p}''') \sigma_2 \psi_{\xi'\alpha'}(p'_0 + p''_0 - p'''_0, \mathbf{p}' + \mathbf{p}'' - \mathbf{p}''')] \times \frac{\{(\zeta^* - 1) [\lambda_0^2 + \lambda_1^2 + 5\lambda_2^2 + \lambda_3^2 + 2(\lambda_0 - \lambda_1 - \lambda_3)\lambda_2 - 2\lambda_0\lambda_3] + \zeta^2 (\lambda_0^2 + \lambda_1^2 + \lambda_2^2 + \lambda_3^2 - 2\lambda_0\lambda_2)\} l}{2\pi v_1 v_2 \zeta^2 \zeta^*}, \quad (\text{A3})$$

$$S_{\xi}^{\lambda_3} = - \int \frac{dp'_0 dp''_0 dp'''_0}{(2\pi)^3} \frac{d^2 \mathbf{p}' d^2 \mathbf{p}'' d^2 \mathbf{p}'''}{(2\pi)^6} [\psi_{\xi\alpha}^\dagger(p'_0, \mathbf{p}') \sigma_3 \psi_{\xi\alpha}(p''_0, \mathbf{p}'') \psi_{\xi'\alpha'}^\dagger(p'''_0, \mathbf{p}''') \sigma_3 \psi_{\xi'\alpha'}(p'_0 + p''_0 - p'''_0, \mathbf{p}' + \mathbf{p}'' - \mathbf{p}''')] \times \frac{\{-\zeta^2 [(\lambda_1 + \lambda_2 - 2\lambda_3)\lambda_3 - \lambda_0\lambda_1] + (\zeta^* - 1)\lambda_0(\lambda_1 - \lambda_2)\} l}{\pi v_1 v_2 \zeta^2 \zeta^*}, \quad (\text{A4})$$

for type-I tilted-Dirac semimetals and

$$S_{\xi}^{\lambda_0} = - \int_{-\infty}^{+\infty} \frac{dp'_0 dp''_0 dp'''_0}{(2\pi)^3} \int \frac{d^2 \mathbf{p}' d^2 \mathbf{p}'' d^2 \mathbf{p}'''}{(2\pi)^6} [\psi_{\xi\alpha}^\dagger(p'_0, \mathbf{p}') \sigma_0 \psi_{\xi\alpha}(p''_0, \mathbf{p}'') \psi_{\xi'\alpha'}^\dagger(p'''_0, \mathbf{p}''') \sigma_0 \psi_{\xi'\alpha'}(p'_0 + p''_0 - p'''_0, \mathbf{p}' + \mathbf{p}'' - \mathbf{p}''')] \times [-(\lambda_0^2 + \lambda_1^2 + \lambda_2^2 + \lambda_3^2)L_3 + 2\lambda_0\lambda_1L_2 + 2\lambda_0\lambda_2L_1], \quad (\text{A5})$$

$$S_{\xi}^{\lambda_1} = \int_{-\infty}^{+\infty} \frac{dp'_0 dp''_0 dp'''_0}{(2\pi)^3} \int \frac{d^2 \mathbf{p}' d^2 \mathbf{p}'' d^2 \mathbf{p}'''}{(2\pi)^6} [\psi_{\xi\alpha}^\dagger(p'_0, \mathbf{p}') \sigma_1 \psi_{\xi\alpha}(p''_0, \mathbf{p}'') \psi_{\xi'\alpha'}^\dagger(p'''_0, \mathbf{p}''') \sigma_1 \psi_{\xi'\alpha'}(p'_0 + p''_0 - p'''_0, \mathbf{p}' + \mathbf{p}'' - \mathbf{p}''')] \times \{2[\lambda_1(\lambda_0 + 2\lambda_1 - 2\lambda_2 - \lambda_3) - \lambda_0\lambda_3]L_1 - (\lambda_0^2 + \lambda_1^2 + \lambda_2^2 + \lambda_3^2)L_2 + 2\lambda_0\lambda_1L_3\}, \quad (\text{A6})$$

$$S_{\xi}^{\lambda_2} = \int_{-\infty}^{+\infty} \frac{dp'_0 dp''_0 dp'''_0}{(2\pi)^3} \int \frac{d^2 \mathbf{p}' d^2 \mathbf{p}'' d^2 \mathbf{p}'''}{(2\pi)^6} [\psi_{\xi\alpha}^\dagger(p'_0, \mathbf{p}') \sigma_2 \psi_{\xi\alpha}(p''_0, \mathbf{p}'') \psi_{\xi'\alpha'}^\dagger(p'''_0, \mathbf{p}''') \sigma_2 \psi_{\xi'\alpha'}(p'_0 + p''_0 - p'''_0, \mathbf{p}' + \mathbf{p}'' - \mathbf{p}''')] \times \{-(\lambda_0^2 + \lambda_1^2 + \lambda_2^2 + \lambda_3^2)L_1 + 2[\lambda_2(\lambda_0 - \lambda_1 + 2\lambda_2 - \lambda_3) - \lambda_0\lambda_3]L_2 + 2\lambda_0\lambda_2L_3\}, \quad (\text{A7})$$

$$S_{\xi}^{\lambda_3} = \int_{-\infty}^{+\infty} \frac{dp'_0 dp''_0 dp'''_0}{(2\pi)^3} \int \frac{d^2 \mathbf{p}' d^2 \mathbf{p}'' d^2 \mathbf{p}'''}{(2\pi)^6} [\psi_{\xi\alpha}^\dagger(p'_0, \mathbf{p}') \sigma_3 \psi_{\xi\alpha}(p''_0, \mathbf{p}'') \psi_{\xi'\alpha'}^\dagger(p'''_0, \mathbf{p}''') \sigma_3 \psi_{\xi'\alpha'}(p'_0 + p''_0 - p'''_0, \mathbf{p}' + \mathbf{p}'' - \mathbf{p}''')] \times \{-2\lambda_0\lambda_1L_1 - 2\lambda_0\lambda_2L_2 + 2(\lambda_1 + \lambda_2 - 2\lambda_3)\lambda_3L_3\}, \quad (\text{A8})$$

for type-II tilted-Dirac semimetals, respectively. Here, the related coefficients are nominated as

$$L_1 = \frac{1}{16\pi^2 v_1 v_2} \int_{\Lambda/s}^{\Lambda} \frac{dE}{(\zeta^2 - 1)^{1/2}} [\mathcal{D}_1(\xi, \zeta) + \mathcal{D}_1(-\xi, \zeta)] + \frac{1}{16\pi^2 v_1 v_2} \int_{-\Lambda}^{-\Lambda/s} \frac{dE}{(\zeta^2 - 1)^{1/2}} [\mathcal{D}_1(-\xi, \zeta) + \mathcal{D}_1(\xi, \zeta)], \quad (\text{A9})$$

$$L_2 = \frac{1}{16\pi^2 v_1 v_2} \int_{\Lambda/s}^{\Lambda} \frac{dE}{(\zeta^2 - 1)^{1/2}} [\mathcal{D}_2(\xi, \zeta) + \mathcal{D}_2(-\xi, \zeta)] + \frac{1}{16\pi^2 v_1 v_2} \int_{-\Lambda}^{-\Lambda/s} \frac{dE}{(\zeta^2 - 1)^{1/2}} [\mathcal{D}_2(-\xi, \zeta) + \mathcal{D}_2(\xi, \zeta)], \quad (\text{A10})$$

$$L_3 = \frac{1}{16\pi^2 v_1 v_2} \int_{\Lambda/s}^{\Lambda} \frac{dE}{(\zeta^2 - 1)^{1/2}} [\mathcal{D}_3(\xi, \zeta) + \mathcal{D}_3(-\xi, \zeta)] + \frac{1}{16\pi^2 v_1 v_2} \int_{-\Lambda}^{-\Lambda/s} \frac{dE}{(\zeta^2 - 1)^{1/2}} [\mathcal{D}_3(-\xi, \zeta) + \mathcal{D}_3(\xi, \zeta)], \quad (\text{A11})$$

with

$$\mathcal{D}_1(\xi, \zeta) = \int_{-\infty}^{\infty} d\theta \frac{(|\zeta| \cosh \theta + \eta \zeta \xi) (\zeta^2 - 1) \sinh^2 \theta}{(\xi \zeta \cosh \theta + 1)^3}, \quad \mathcal{D}_1(-\xi, \zeta) = \int_{-\infty}^{\infty} d\theta \frac{(|\zeta| \cosh \theta - \eta \zeta \xi) (\zeta^2 - 1) \sinh^2 \theta}{(-\xi \zeta \cosh \theta + 1)^3}, \quad (\text{A12})$$

$$\mathcal{D}_2(\xi, \zeta) = \int_{-\infty}^{\infty} d\theta \frac{(|\zeta| \cosh \theta + \eta \zeta \xi) (\xi \zeta + \cosh \theta)^2}{(\xi \zeta \cosh \theta + 1)^3}, \quad \mathcal{D}_2(-\xi, \zeta) = \int_{-\infty}^{\infty} d\theta \frac{(|\zeta| \cosh \theta - \eta \zeta \xi) (-\xi \zeta + \cosh \theta)^2}{(-\xi \zeta \cosh \theta + 1)^3}, \quad (\text{A13})$$

$$\mathcal{D}_3(\xi, \zeta) = \int_{-\infty}^{\infty} d\theta \frac{(|\zeta| \cosh \theta + \eta \zeta \xi)}{(\xi \zeta \cosh \theta + 1)}, \quad \mathcal{D}_3(-\xi, \zeta) = \int_{-\infty}^{\infty} d\theta \frac{(|\zeta| \cosh \theta - \eta \zeta \xi)}{(-\xi \zeta \cosh \theta + 1)}. \quad (\text{A14})$$

In order to calculate the coefficients \mathcal{D}_i with $i = 1, 2, 3$ for type-II tilted Dirac fermions, one needs to introduce an UV cutoff in θ , which is designated as θ^Λ and determined by the size of first Brillouin Zone [35, 36]. Following the strategy advocated in Ref. [36], we assume the maximum value of $|p_2|$ is related to the lattice spacing a_0 at the scale l , namely $|p_2|_{\max} = \pi/a_0$, and then arrive at for a specific value of E by resorting to the Eq. (11),

$$\tilde{p}_2 = v_2 p_2 = \frac{|E| \sinh \theta_\Lambda}{\sqrt{\zeta^2 - 1}} \approx \frac{|E| e^{\theta_\Lambda}}{2\sqrt{\zeta^2 - 1}} \approx \frac{v_2 \pi}{a_0} \equiv D, \quad (\text{A15})$$

with $\Lambda = O(D)$ (the basic results are insensitive to the ratio D/Λ [35, 36]). This yields to

$$e^{\theta_\Lambda} = \frac{2\sqrt{\zeta^2 - 1}D}{|E|}. \quad (\text{A16})$$

Exploiting this approach and performing several calculations eventually give rise to the compact one-loop corrections for type-II tilted Dirac fermions,

$$S_\xi^{\lambda_0} = \int_{-\infty}^{+\infty} \frac{dp'_0 dp''_0 dp'''_0}{(2\pi)^3} \int \frac{d^2 \mathbf{p}' d^2 \mathbf{p}'' d^2 \mathbf{p}'''}{(2\pi)^6} [\psi_{\xi\alpha}^\dagger(p'_0, \mathbf{p}') \sigma_0 \psi_{\xi\alpha}(p''_0, \mathbf{p}'') \psi_{\xi'\alpha'}^\dagger(p'''_0, \mathbf{p}''') \sigma_0 \\ \times \psi_{\xi'\alpha'}(p'_0 + p''_0 - p'''_0, \mathbf{p}' + \mathbf{p}'' - \mathbf{p}''')] \frac{2\lambda_0 \lambda_1 \zeta^* l}{\pi^2 \zeta |\zeta| v_1 v_2}, \quad (\text{A17})$$

$$S_\xi^{\lambda_1} = \int_{-\infty}^{+\infty} \frac{dp'_0 dp''_0 dp'''_0}{(2\pi)^3} \int \frac{d^2 \mathbf{p}' d^2 \mathbf{p}'' d^2 \mathbf{p}'''}{(2\pi)^6} [\psi_{\xi\alpha}^\dagger(p'_0, \mathbf{p}') \sigma_1 \psi_{\xi\alpha}(p''_0, \mathbf{p}'') \psi_{\xi'\alpha'}^\dagger(p'''_0, \mathbf{p}''') \sigma_1 \\ \times \psi_{\xi'\alpha'}(p'_0 + p''_0 - p'''_0, \mathbf{p}' + \mathbf{p}'' - \mathbf{p}''')] \frac{(\lambda_0^2 + \lambda_1^2 + \lambda_2^2 + \lambda_3^2) \zeta^* l}{2\pi^2 \zeta |\zeta| v_1 v_2}, \quad (\text{A18})$$

$$S_\xi^{\lambda_2} = \int_{-\infty}^{+\infty} \frac{dp'_0 dp''_0 dp'''_0}{(2\pi)^3} \int \frac{d^2 \mathbf{p}' d^2 \mathbf{p}'' d^2 \mathbf{p}'''}{(2\pi)^6} [\psi_{\xi\alpha}^\dagger(p'_0, \mathbf{p}') \sigma_2 \psi_{\xi\alpha}(p''_0, \mathbf{p}'') \psi_{\xi'\alpha'}^\dagger(p'''_0, \mathbf{p}''') \sigma_2 \\ \times \psi_{\xi'\alpha'}(p'_0 + p''_0 - p'''_0, \mathbf{p}' + \mathbf{p}'' - \mathbf{p}''')] \frac{2[\lambda_0 \lambda_3 - \lambda_2 (\lambda_0 - \lambda_1 + 2\lambda_2 - \lambda_3)] \zeta^* l}{\pi^2 \zeta |\zeta| v_1 v_2}, \quad (\text{A19})$$

$$S_\xi^{\lambda_3} = \int_{-\infty}^{+\infty} \frac{dp'_0 dp''_0 dp'''_0}{(2\pi)^3} \int \frac{d^2 \mathbf{p}' d^2 \mathbf{p}'' d^2 \mathbf{p}'''}{(2\pi)^6} [\psi_{\xi\alpha}^\dagger(p'_0, \mathbf{p}') \sigma_3 \psi_{\xi\alpha}(p''_0, \mathbf{p}'') \psi_{\xi'\alpha'}^\dagger(p'''_0, \mathbf{p}''') \sigma_3 \\ \times \psi_{\xi'\alpha'}(p'_0 + p''_0 - p'''_0, \mathbf{p}' + \mathbf{p}'' - \mathbf{p}''')] \frac{2\lambda_0 \lambda_2 \zeta^* l}{\pi^2 \zeta |\zeta| v_1 v_2}, \quad (\text{A20})$$

where the coefficients ζ^* and ζ^* are introduced in Eq. (24).

-
- [1] K. S. Novoselov, A. K. Geim, S. V. Morozov, D. Jiang, Y. Zhang, S. V. Dubonos, I. V. Grigorieva, and A. A. Firsov, *Science* **306**, 666 (2004).
[2] K. S. Novoselov, A. K. Geim, S. V. Morozov, D. Jiang, M. I. Katsnelson, I. V. Grigorieva, S. V. Dubonos, and A. A. Firsov, *Nature* **438**, 197 (2005).

- [3] A. H. Castro Neto, F. Guinea, N. M. R. Peres, K. S. Novoselov, and A. K. Geim, *Rev. Mod. Phys.* **81**, 109 (2009).
[4] N. M. R. Peres, *Rev. Mod. Phys.* **82**, 2673 (2010).
[5] A. A. Burkov and L. Balents, *Phys. Rev. Lett.* **107**, 127205 (2011).

- [6] K. -Y. Yang, Y. -M. Lu, and Y. Ran, Phys. Rev. B **84**, 075129 (2011).
- [7] X. Wan, A. M. Turner, A. Vishwanath, and S. Y. Savrasov, Phys. Rev. B **83**, 205101 (2011).
- [8] X. Huang, et al., Phys. Rev. X **5**, 031023 (2015).
- [9] S. -Y. Xu, I. Belopolski, N. Alidoust, M. Neupane, G. Bian, C. Zhang, R. Sankar, G. Chang, Z. Yuan, C. -C. Lee, et al., Science **349**, 613 (2015).
- [10] S. -Y. Xu, N. Alidoust, I. Belopolski, Z. Yuan, G. Bian, T. -R. Chang, H. Zheng, V. N. Strocov, D. S. Sanchez, G. Chang, et al., Nat. Phys. **11**, 748 (2015).
- [11] B. Q. Lv, N. Xu, H. M. Weng, J. Z. Ma, P. Richard, X. C. Huang, L. X. Zhao, G. F. Chen, C. E. Matt, F. Bisti, V. N. Strocov, J. Mesot, Z. Fang, X. Dai, T. Qian, M. Shi, and H. Ding, Nat. Phys. **11**, 724 (2015).
- [12] H. Weng, C. Fang, Z. Fang, B. A. Bernevig, and X. Dai, Phys. Rev. X **5**, 011029 (2015).
- [13] B. Roy, R. J. Slager, and V. Juričić, Phys. Rev. X **8**, 031076 (2018).
- [14] O. Vafek and A. Vishwanath, Annu. Rev. Condens. Matter Phys. **5**, 83 (2014).
- [15] T. O. Wehling, A. M. Black-Schaffer, and A. V. Balatsky, Adv. Phys. **63**, 1 (2014).
- [16] Z. -J. Wang, Y. Sun, X. -Q. Chen, C. Franchini, G. Xu, H. -M. Weng, X. Dai, and Z. Fang, Phys. Rev. B **85**, 195320 (2012).
- [17] S. -M. Young, S. Zaheer, J. -C. Teo, C. -L. Kane, E. -J. Mele and A. -M. Rappe, Phys. Rev. Lett. **108**, 140405 (2012).
- [18] J. -A. Steinberg, S. -M. Young, S. Zaheer, C. -L. Kane, E. -J. Mele, and A. -M. Rappe, Phys. Rev. Lett. **112**, 036403 (2014).
- [19] Z. K. Liu et al., Nat. Mater. **13**, 677 (2014).
- [20] Z. K. Liu et al., Science **343**, 864 (2014).
- [21] J. Xiong, S. K. Kushwaha, T. Liang, J. W. Krizan, M. Hirschberger, W. Wang, R. J. Cava, and N. P. Ong, Science **350**, 413 (2015).
- [22] R. Roy, Phys. Rev. B **79**, 195322 (2009).
- [23] B. Roy, S. Das Sarma, Phys. Rev. B **94**, 115137 (2016); B. Roy, Y. Alavirad, and J. D. Sau, Phys. Rev. Lett. **94**, 227002 (2017); B. Roy, R. -J. Slager, and V. Juricic, arXiv: 1610.08973 (2016); B. Roy, V. Juricic, and S. Das Sarma, Sci. Rep. **6**, 32446 (2016).
- [24] H. -H. Lai, B. Roy, and P. Goswami, arXiv: 1409.8675 (2014); P. Goswami, B. Roy, and S. Das Sarma, Phys. Rev. B **95**, 085120 (2017); A. L. Szabo, R. Moessner, and B. Roy, arXiv:1811.12415 (2018); B. Roy, S. A. Akbar Ghorashi, M. S. Foster, and A. H. Nevidomskyy, Phys. Rev. B **99**, 054505 (2019).
- [25] L. Savary, J. Ruhman, J. W. F. Venderbos, L. Fu, and P. A. Lee, Phys. Rev. B **96**, 214514 (2017).
- [26] L. Savary, E. -G. Moon and L. Balents, Phys. Rev. X **4**, 041027 (2014); H. Oh, S. Lee, Y. -B. Kim, and E. -G. Moon, arXiv: cond-mat.str-el/1811.00021 (2018).
- [27] P. Dietl, F. Piechon, and G. Montambaux, Phys. Rev. Lett. **100**, 236405 (2008); G. Montambaux, F. Piéchon, J. -N. Fuchs, and M. O. Goerbig, Phys. Rev. B **80**, 153412 (2009); P. Delplace and G. Montambaux, Phys. Rev. B **82**, 035438 (2010); L. -K. Lim, J. -N. Fuchs, and Gilles Montambaux, Phys. Rev. Lett. **108**, 175303 (2012).
- [28] A. Altland and B. Simons, *Condensed Matter Field Theory* (Cambridge University Press, Cambridge, 2006).
- [29] M. Z. Hasan and C. L. Kane, Rev. Mod. Phys. **82**, 3045 (2010).
- [30] X. -L. Qi and S. -C. Zhang, Rev. Mod. Phys. **83**, 1057 (2011).
- [31] B. Q. Lv, H. M. Weng, B. B. Fu, X. P. Wang, H. Miao, J. Ma, P. Richard, X. C. Huang, L. X. Zhao, G. F. Chen, Z. Fang, X. Dai, T. Qian, and H. Ding, Phys. Rev. X **5**, 031013 (2015).
- [32] L. Yang, Z. Liu, Y. Sun, H. Peng, H. Yang, T. Zhang, B. Zhou, Y. Zhang, Y. Guo, M. Rahn, et al., Nature Physics **11**, 728 (2015).
- [33] C. Shekhar, A. K. Nayak, Y. Sun, M. Schmidt, M. Nicklas, I. Leermakers, U. Zeitler, W. Schnelle, J. Grin, C. Felser, et al., Nature Physics **11**, 645 (2015).
- [34] N. Xu, H. M. Weng, B. Q. Lv, C. E. Matt, J. Park, F. Bisti, V. N. Strocov, D. Gawryluk, E. Pomjakushina, K. Conder, N. C. Plumb, M. Radovic, G. Aútes, O. V. Yazyev, Z. Fang, X. Dai, T. Qian, J. Mesot, H. Ding, and M. Shi, Nat. Commun. **7**, 11006 (2016).
- [35] Y. -W. Lee and Y. -L, Phys. Rev. B **97**, 035141 (2018).
- [36] Y. -L. Lee and Y. -W. Lee, Phys. Rev. B **100**, 075156 (2019).
- [37] S. A. Jafari, Phys. Rev. B **100**, 045144 (2019).
- [38] S. Katayama, A. Kobayashi, and Y. Suzumura, J. Phys. Soc. Jpn. **75**, 054705 (2006).
- [39] A. Kobayashi, S. Katayama, Y. Suzumura, and H. Fukuyama, J. Phys. Soc. Jpn. **76**, 034711 (2007).
- [40] M. O. Goerbig, J. -N. Fuchs, G. Montambaux, and F. Piéchon, Phys. Rev. B **78**, 045415 (2008).
- [41] A. A. Soluyanov, D. Gresch, Z. J. Wang, Q. S. Wu, M. Troyer, X. Dai, and B. A. Bernevig, Nature (London) **527**, 495 (2015).
- [42] Y. Xu, F. Zhang, and C. Zhang, Phys. Rev. Lett. **115**, 265304 (2015).
- [43] Y. Xu and L. -M. Duan, Phys. Rev. A **94**, 053619 (2016).
- [44] S. A. Jafari, Eur. Phys. J. B **68**, 537 (2009); Z. Jalali-Mola and S. A. Jafari, Phys. Rev. B **100**, 075113 (2019); T. Farajollahpour, Z. Faraei, and S. A. Jafari, Phys. Rev. B **100**, 045144 (2019).
- [45] H. J. Noh, J. Jeong, E. J. Cho, K. Kim, B. I. Min, and B. G. Park, Phys. Rev. Lett. **119**, 016401 (2017).
- [46] F. C. Fei, X. Y. Bo, R. Wang, B. Wu, J. Jiang, D. Z. Fu, M. Gao, H. Zheng, Y. L. Chen, X. F. Wang, H. J. Bu, F. Q. Song, X. G. Wang, B. G. Wang, and G. H. Wang, Phys. Rev. B **96**, 041201(R) (2017).
- [47] M. Z. Yan, H. Q. Huang, K. N. Zhang, E. Wang, W. Yao, K. Deng, G. L. Wan, H. Y. Zhang, M. Arita, H. T. Yang, Z. Sun, H. Yao, Y. Wu, S. S. Fan, W. H. Duan, and S. Y. Zhou, Nat. Commun. **8**, 257 (2017).
- [48] C. Shekhar, A. K. Nayak, Y. Sun, M. Schmidt, M. Nicklas, I. Leermakers, U. Zeitler, Y. Skourski, J. Wosnitza, Z. Liu, Y. Chen, W. Schnelle, H. Borrmann, Y. Grin, C. Felser, and B. Yan, Nature Physics **11**, 3372 (2015).
- [49] S. A. Parameswaran, T. Grover, D. A. Abanin, D. A. Pesin, and A. Vishwanath, Phys. Rev. X **4**, 031035 (2014).
- [50] A. C. Potter, I. Kimchi, and A. Vishwanath, Nature Communications **5**, 6161 (2014).
- [51] Y. Baum, E. Berg, S. A. Parameswaran, and A. Stern, Phys. Rev. X **5**, 041046 (2015).
- [52] F. Arnold, C. Shekhar, S. -C. Wu, Y. Sun, R. D. dos Reis, N. Kumar, M. Naumann, M. O. Ajeesh, M. Schmidt, A. G. Grushin, J. H. Bardarson, M. Baenitz, D. Sokolov, H. Borrmann, M. Nicklas, C. Felser, E. Hassinger, and B. Yan, Nature Communications **7**, 11615 (2016).

- [53] C. -L. Zhang, S. -Y. Xu, I. Belopolski, Z. Yuan, Z. Lin, B. Tong, G. Bian, N. Alidoust, C. -C. Lee, S. -M. Huang, T. R. Chang, G. Chang, C. -H. Hsu, H. -T. Jeng, M. Neupane, D. S. Sanchez, H. Zheng, J. Wang, H. Lin, C. Zhang, H. -Z. Lu, S. -Q. Shen, T. Neupert, M. Zahid Hasan, and S. Jia, *Nature Communications* **7**, 10735 (2016).
- [54] F. Detassis, L. Fritz, and S. Grubinskas, *Phys. Rev. B* **96**, 195157 (2017).
- [55] T. S. Sikkenk and L. Fritz, *Phys. Rev. B* **100**, 085121 (2019).
- [56] Z. Jalali-Mola and S. A. Jafari, *Phys. Rev. B* **98**, 195415 (2018).
- [57] Z. -K. Yang, J. -R. Wang, and G. -Z. Liu, *Phys. Rev. B* **98**, 195123 (2018).
- [58] M. Trescher, B. Sbierski, P. W. Brouwer, and E. J. Bergholtz, *Phys. Rev. B* **91**, 115135 (2015).
- [59] I. Proskurin, M. Ogata, and Y. Suzumura, *Phys. Rev. B* **91**, 195413 (2015).
- [60] T. E. O'Brien, M. Diez, and C. W. J. Beenakker, *Phys. Rev. Lett.* **116**, 236401 (2016); Z. M. Yu, Y. Yao, and S. A. Yang, *Phys. Rev. Lett.* **117**, 077202 (2016); M. Udagawa and E. J. Bergholtz, *Phys. Rev. Lett.* **117**, 086401 (2016); S. Tchoumakov, M. Civelli, and M. O. Goerbig, *Phys. Rev. Lett.* **117**, 086402 (2016).
- [61] A. A. Zyuzin and R. P. Tiwari, *JETP Lett.* **103**, 717 (2016); J. F. Steiner, A. V. Andreev, and D. A. Pesin, *Phys. Rev. Lett.* **119**, 036601 (2017).
- [62] Y. Ferreira, A. A. Zyuzin, and J. H. Bardarson, *Phys. Rev. B* **96**, 115202 (2017); S. Saha and S. Tewari, *Eur. Phys. J. B* **91**, 4 (2018).
- [63] M. Alidoust and K. Halterman, *arXiv: 1906.05382* (2019).
- [64] S. Das Sarma, S. Adam, E. H. Hwang, and E. Rossi, *Rev. Mod. Phys.* **83**, 407 (2011).
- [65] V. N. Kotov, B. Uchoa, V. M. Pereira, F. Guinea and A. H. Castro Neto, *Rev. Mod. Phys.* **84**, 1067 (2012).
- [66] M. I. Katsnelson, *Phys. Rev. B* **74**, 201401(R) (2006).
- [67] V. Cvetkovic, R. E. Throckmorton, and O. Vafek, *Phys. Rev. B* **86**, 075467 (2012); J. M. Murray, O. Vafek, *Phys. Rev. B* **89**, 201110(R) (2014).
- [68] I. F. Herbut, L. Janssen, *Phys. Rev. Lett.* **113**, 106401 (2014); L. Janssen, I. F. Herbut, *Phys. Rev. B* **89**, 205403 (2014); L. Janssen, I. F. Herbut, *Phys. Rev. B* **92**, 045117 (2015).
- [69] I. Boettcher, I. F. Herbut, *Phys. Rev. B* **93**, 205138 (2016); I. F. Herbut, *Phys. Rev. Lett.* **97**, 146401 (2006).
- [70] J. Wang, C. Ortix, J. van den Brink, and D. V. Efremov, *Phys. Rev. B* **96**, 201104(R) (2017).
- [71] J. Wang, *J. Phys. Condens. Matter* **30**, 125401 (2018); Y. -M. Dong, D. -X. Zheng, and J. Wang, *J. Phys. Condens. Matter* **31**, 275601 (2019); J. Wang, *Eur. Phys. J. B* **92**, 102 (2019).
- [72] K. G. Wilson, *Rev. Mod. Phys.* **47**, 773 (1975).
- [73] J. Polchinski, *arXiv: hep-th/9210046* (1992).
- [74] R. Shankar, *Rev. Mod. Phys.* **66**, 129 (1994).
- [75] N. Nandkishore, J. Maciejko, D. A. Huse, and S. L. Sondhi, *Phys. Rev. B* **87**, 174511 (2013).
- [76] I. -D. Potirniche, J. Maciejko, R. Nandkishore, and S. L. Sondhi, *Phys. Rev. B* **90**, 094516 (2014).
- [77] J. Wang, P. -L. Zhao, J. -R. Wang, and G. -Z. Liu, *Phys. Rev. B* **95**, 054507 (2017).
- [78] Y. Huh, S. Sachdev, *Phys. Rev. B* **78**, 064512 (2008); E. -A. Kim, M. J. Lawler, P. Oreto, S. Sachdev, E. Fradkin, and S. A. Kivelson, *Phys. Rev. B* **77**, 184514 (2008).
- [79] J. -H. She, J. Zaanen, A. R. Bishop, and A. V. Balatsky, *Phys. Rev. B* **82**, 165128 (2010).
- [80] J. Wang, G. -Z. Liu, and H. Kleinert, *Phys. Rev. B* **83**, 214503 (2011).
- [81] E. M. Lifshitz, *J. Phys. (Moscow)* **6**, 61 (1942).
- [82] I. E. Dzyaloshinski, *Zh. Eksp. Teor. Fiz.* **46**, 1420 (1964).
- [83] M. D. Goshen, S. and S. Shtrikman, *Int. J. Magn.* **6**, 221 (1974).
- [84] R. M. Hornreich, M. Luban, and S. Shtrikman, *Phys. Rev. Lett.* **35**, 1678 (1975).
- [85] B. Roy and M. S. Foster, *Phys. Rev. X* **8**, 011049 (2018).
- [86] B. Roy, *Phys. Rev. B* **96**, 041113(R) (2017).
- [87] C. J. Halboth and W. Metzner, *Phys. Rev. Lett.* **85**, 5162 (2000).
- [88] A. V. Chubukov, M. Khodas, and R. M. Fernandes, *Phys. Rev. X* **6**, 041045 (2016).

